Investigating the VLBI Scale Behaviour

How is the VLBI Technique Defined Scale Affected by the Session Network Components?

Master's thesis in Wireless, Photonics and Space Engineering

FREDRIK NYSTRÖM LINDÉ

DEPARTMENT OF SPACE, EARTH AND ENVIRONMENT

CHALMERS UNIVERSITY OF TECHNOLOGY
Gothenburg, Sweden 2022
www.chalmers.se

Master's thesis 2022

Investigating the VLBI Scale Behaviour

How is the VLBI Technique Defined Scale Affected by the Session Network Components?

FREDRIK NYSTRÖM LINDÉ

Department of Space, Earth and Environment
Division of Geoscience and Remote Sensing
Chalmers University of Technology
Gothenburg, Sweden 2022

Investigating the VLBI Scale Behaviour
How is the VLBI Technique Defined Scale Affected by the Session Network Components?
FREDRIK NYSTRÖM LINDÉ

Supervisors: Karine Le Bail, Department of Space, Earth and Environment
Rüdiger Haas, Department of Space, Earth and Environment

Examiner: Karine Le Bail, Department of Space, Earth and Environment

Master's Thesis 2022
Department of Space, Earth and Environment
Division of Geoscience and Remote Sensing
Chalmers University of Technology
SE-412 96 Gothenburg
Telephone +46 31 772 1000

Typeset in LaTeX
Printed by Chalmers Reproservice
Gothenburg, Sweden 2022

Investigating the VLBI Scale Behaviour
How is the VLBI Technique Defined Scale Affected by the Session Network Components?
FREDRIK NYSTRÖM LINDÉ
Department of Space, Earth and Environment
Chalmers University of Technology

Abstract

In preparation of the latest realisation of the International Terrestrial Reference Frame (ITRF), the ITRF2020, the Very Long Baseline Interferometry (VLBI) solution displayed some strange behaviour in regards to its scale factor. Some clear reason for what can only be described as a scale drift, has yet to be observed, while several possible reasons have been discussed. In this thesis we aim to investigate the VLBI scale factor based on the Onsala Space Observatory (OSO) individual VLBI solution to find any obvious correlation between the scale drift and the components of a VLBI session network. A large portion of the work was spent developing a toolbox in MATLAB to analyse VLBI solutions, and to estimate the seven Helmert parameters for transformation between different terrestrial reference frames (TRFs). With these tools we looked at the effects of simulating an erroneous uplift model by artificially adding motion to stations distributed around the globe. The results indicated that the necessary uplift error to cause such a drift would have to be in the magnitude of cm/yr. Then we also used the software package ASCOT to reprocess global VLBI solutions while excluding stations that had experienced different technical issues, or on the hypothesis that network volume or distribution would have an effect. The results of excluding stations with technical issues proved most promising in reducing the scale drift, while removing stations based on the network distribution seemed to have the opposite effect. Our results indicate that the VLBI scale drift problem seem to be the result of a combination of factors, and there are surely other aspects at play as well.

Keywords: VLBI, IVS, ITRF, scale factor, OSO, space geodesy, Helmert parameters.

Acknowledgements

First and foremost, I would like to express my gratitude towards my supervisors Karine Le Bail and Rüdiger Haas. I very much appreciate you both staying patient with me during the process, as well as your valuable feedback throughout. It has been an incredible journey where I have learnt not only all about the technical aspects, but also the practical aspects of such an undertaking. Both of your valuable inputs have been essential for this thesis' success.

I would also like to give thanks to Tobias Nilsson at Lantmäteriet for providing us with all the data to work with; extending his knowledge about the VLBI analysis, and for helping us troubleshoot ASCOT when we encountered issues. On a similar note I must also thank Armin Corbin for the ASCOT workshops, and guiding use through the software package.

Lastly, I want to extend my thanks to Periklis Diamantidis, a PhD Student at our division, for his very helpful advice and for telling me to stop worrying about every singly tiny detail. And of course Laurent Métivier at the IGN-IPGP, for helping us to make sure that our post-seismic corrections were indeed correct.

Fredrik Nyström Lindé, Gothenburg, June 2022

Contents

List of Figures

List of Tables

List of Acronyms

AC	Analysis Center
ASCOT	Analysis, Scheduling and Combination Toolbox
CRF	Celestial Reference Frame
CRS	Celestial Reference System
DORIS	Doppler Orbitography and Radiopositioning Integrated by Satellite
EOP	Earth Orientation Parameter
ETRS89	European Terrestrial Reference System 1989
GNSS	Global Satellite Navigation Systems
GRS80	Geodetic Reference System 1980
ICRF	International Celestial Reference Frame
ICRS	International Celestial Reference System
IDS	International DORIS Service
IERS	International Earth Rotation and Reference Systems Service
IGS	International GNSS Service
ILRS	International Laser Ranging Service
ITRF	International Terrestrial Reference Frame
ITRS	International Terrestrial Reference System
IVS	International VLBI Service for Geodesy & Astrometry
NNR	No-Net-Rotation
NNT	No-Net-Translation
OSO	Onsala Space Observatory
ppb	Parts-per-billion
ppm	Parts-per-million
SINEX	Solution INdependent EXchange
SLR	Satellite Laser Ranging
TRF	Terrestrial Reference Frame
TRS	Terrestrial Reference System
VLBI	Very Long Baseline Interferometry

1
Introduction

In today's world we make much use of, and rely heavily upon, the ability to accurately determine positions. Whether it is science, agriculture, land surveying, or simply finding the nearest store around the corner, we expect to have accurate coordinates readily available. But these coordinates or positions must always be given *in relation to* a set reference frame. While there exists both global and regional reference frames, the International Terrestrial Reference Frame (ITRF) is the most accurate realisation of the Terrestrial Reference Systems (TRSs).

Every few years an updated realisation of the ITRS, that is the ITRF solutions, is produced with the inclusion of new data, from the combination of geodetic products of the four major space-geodetic techniques. These are the Global Satellite Navigation Systems (GNSS), Satellite Laser Ranging (SLR), Doppler Orbitography Radiopositioning Integrated by Satellite (DORIS), and Very Long Baseline Interferometry (VLBI). None of these techniques are able to accurately realise the ITRS on their own, and they each have their own strengths and weaknesses. By combining the techniques through the use of globally distributed co-location sites, that is sites with two or more space-geodetic instruments operating very close to each other, the strengths of each technique is able to be utilised to a larger extent.

With every new ITRF solution, the newest iteration is usually validated by comparing it to past realisations of the ITRF. This can be done by performing a so-called Helmert transformation which is a similarity transformation of seven parameters, three translation components, one scale factor, and three rotation angles. The scale factor in particular is determined from the products of the VLBI and SLR techniques. However, during investigations by Altamimi et al. (2022) in preparation for the upcoming model ITRF2020, the time series of the VLBI scale beginning around 2014 appeared to show what can only be described as a positive drift. This was alarming because one of the major contributions from the International VLBI Service for Geodesy & Astronometry (IVS, see Nothnagel et al. 2017) is this scale factor. While only appearing as a visual phenomena at first, it was deemed appropriate to investigate this behaviour of the scale factor and attempt to find out why it might be drifting or experiencing larger scatter.

This Master's thesis project is aimed at investigating this scale behaviour as observed in the time series of the VLBI solutions. Several possible reasons for this behaviour have been brought into discussion, and this project focuses on investigating some correlation between the scale and the components of the VLBI station network. This is accomplished by reprocessing individual VLBI solutions using existing software, but perhaps more importantly through the development of a VLBI session analysis toolbox in MATLAB. This work would not have been possible without the enormous help and effort from the Division of Geoscience and Remote Sensing at the Onsala Space Observatory (OSO), the Swedish National Facility for Radio Astronomy, and Lantmäteriet - the Swedish Mapping, Cadastral, and Land Registration authority.

As a final note, because this work is based on comparing different solutions of the ITRF, it should be made clear which version has been used. At the start of this project in January of 2022 the last published iteration was the ITRF2014, and thus all work, analysis and preliminary results from this project are based on the ITRF2014 as the reference frame for comparison. Towards the end of this project, in April of 2022, the ITRF2020 solution was published. While the work was not able to be moved to the ITRF2020 in time, it should be noted that the VLBI scale behaviour had still not been resolved with no clear observations as to what might be causing it.

2

Background

This chapter aims to give the reader a basic understanding of *terrestrial reference systems* and *terrestrial reference frames*. These concepts are then put into context through the ITRS and ITRF, and briefly discusses how these can be used in practice. Lastly the VLBI technique is discussed in more detail, as well as the VLBI contribution to the ITRF coordinated by the IVS.

2.1 Understanding a TRS and TRF

Geodesy at its core relies on accurately determining positions of points on the Earth, based on some coordinate reference system. Whether it is land surveying or mapping, or tracking for instance crustal motion or polar motion, these points must be determined in relation to some form of spatial reference system. Such a coordinate system viewed from the Earth is called a Terrestrial Reference System (TRS), and its corresponding physical realisation is called a Terrestrial Reference Frame (TRF). Before continuing further it is important to understand the fundamental difference between a TRS and TRF. A TRS should be thought of as the theoretical definition of a coordinate system, which is distinguished from its physical realisation. The TRS is the set of regulations, conventions, and mathematical models that are used to define the properties of a coordinate system such as origin, scale, orientation, and also how these properties change over time.

In practice a TRS defines a three-dimensional reference frame around the Earth that co-rotates with it, as opposed to a celestial reference system (CRS) that is fixed to the stars in space (Altamimi et al. 2001). In the context of this project, only geocentric systems are considered, that is with the point of origin close to the center-of-mass (geocenter) of the entire Earth system which includes the entire solid Earth and its atmosphere. Furthermore, as described by Petit and Luzum (2010) and in Angermann et al. (2013), the coordinate system is made up of three right-handed, orthogonal base vectors of equal length. The length of the unit vectors defines its scale and should be close to an SI meter (Petit and Luzum 2010). The orientation of the reference system is said to be equatorial and should be oriented so that the z axis is in the direction of the poles, and thus (considering Cartesian coordinates) the x and y axes both pass through the Equator due to them being orthogonal. Additionally, as seen in Figure 2.1, the x axis passes through the Greenwich meridian, or longitude 0° in a geographic coordinate system (Petit and Luzum 2010).

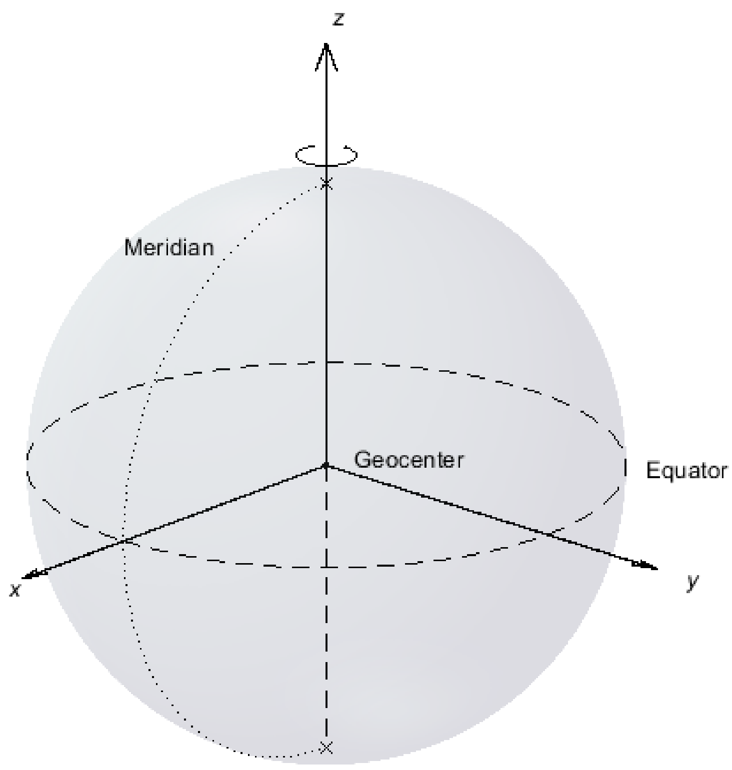

Figure 2.1: A conventional TRS with its origin at the Earth's geocenter, z axis through the poles, and x and y axes through the Equatorial plane.

With an ideal TRS defined, the actual physical realisation of the system is what is called a TRF. A TRF consists of a set of physical points whose coordinates have been precisely determined. The realisation is done using any of the four major space-geodetic techniques, and the physical points on the Earth's surface correspond to the network of ground stations, receivers, or equipment for each respective technique. That is, radio telescopes for VLBI, laser telescopes for SLR, and receiver antennas for GNSS that all perform various kinds of measurements. The DORIS technique works a bit differently and instead only emits a signal from each beacon. In principle this means that each of the four techniques compute and realise their own model of a TRF, based on their own network of ground stations. Furthermore, such a TRF is only valid for the reference epoch, or moment in time, of the measurements.

Because of many different applications for reference frames, there are not only global realisations of a TRS, but there can also be local or regional realisations. One such example is the European Terrestrial Reference System 1989 (ETRS89) which is a reference system local to the Eurasian Plate (Bruyninx et al. 2017). This reference system can in turn be realised even more locally, for instance as the Swedish reference frame SWEREF 99 (Jivall and Lidberg 2000). The idea for more regional reference systems is so that coordinates will not change due to continental drift, but also because the Earth is not a perfect ellipsoid and each region around the globe might be best approximated by an ellipsoid other than the global estimate.

2.2 Helmert Transformation Between TRFs

Sometimes it is necessary to transform coordinates between two different reference frames. The standard approach to do this is to apply a seven parameter similarity transformation, often called the Helmert transformation (Petit and Luzum 2010). The seven parameters consist of three translation components (usually denoted as T_x, T_y, and T_z), one scale factor (often denoted D), and three rotation angles (denoted as rotation around each respective axis as R_x, R_y, and R_z). To also describe the time evolution between two reference frames the first time derivative of each of the seven parameters is used, for a total of fourteen parameters.

Such a transformation is necessary because despite each physical point being fixed at a given moment in time (the reference epoch), be it an antenna phase center, or some ground marker, the actual coordinates of this point in different reference frames will deviate slightly. This is illustrated in Figure 2.2 which displays the first seven Helmert parameters necessary to derive the positions of a point in two reference frames. The translation parameters could be considered as the distance to travel, and the rotation parameters as the rotation around each of the axes, to arrive at the same point in the second reference frame.

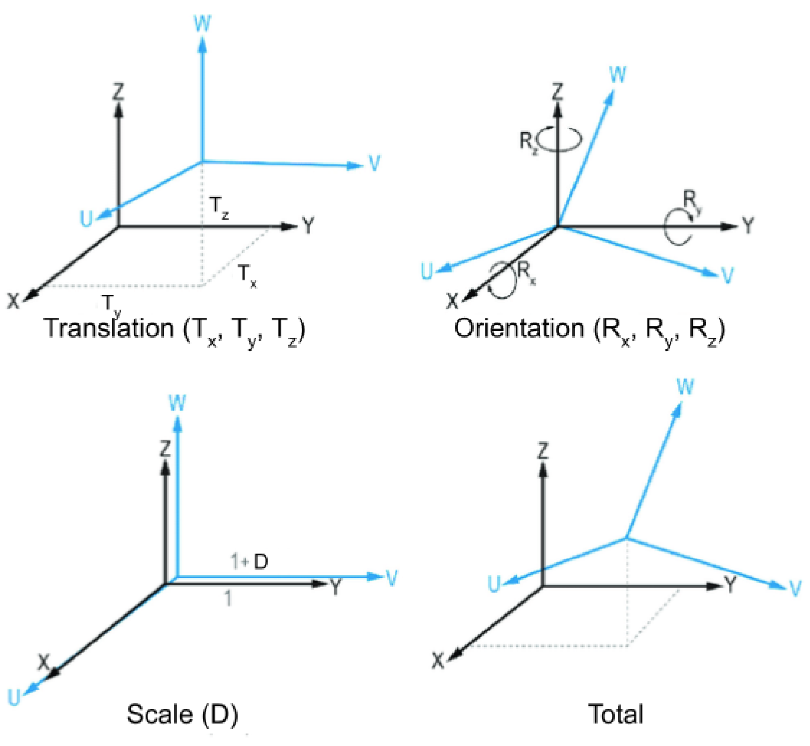

Figure 2.2: Visualisation of each of the seven Helmert parameters and the total transformation. (Original image by: Malys et al. 2021)

By applying the seven (or fourteen) Helmert parameters the transformation between two frames can be expressed in either position, time evolution, or both. However, note that the parameters to transform from one reference frame to another are unique to that set of frames. The transformation formula for both the set of positions and rates between two reference frames (from frame 1 to frame 2) can be written as (Altamimi et al. 2017b)

$$
\begin{cases}
\begin{pmatrix} x_2 \\ y_2 \\ z_2 \end{pmatrix} = \begin{pmatrix} x_1 \\ y_1 \\ z_1 \end{pmatrix} + T + D \begin{pmatrix} x_1 \\ y_1 \\ z_1 \end{pmatrix} + R \begin{pmatrix} x_1 \\ y_1 \\ z_1 \end{pmatrix}, \\[2ex]
\begin{pmatrix} \dot{x}_2 \\ \dot{y}_2 \\ \dot{z}_2 \end{pmatrix} = \begin{pmatrix} \dot{x}_1 \\ \dot{y}_1 \\ \dot{z}_1 \end{pmatrix} + \dot{T} + \dot{D} \begin{pmatrix} x_1 \\ y_1 \\ z_1 \end{pmatrix} + \dot{R} \begin{pmatrix} x_1 \\ y_1 \\ z_1 \end{pmatrix},
\end{cases}
\tag{2.1}
$$

where the coordinates x, y, and z in the left-hand side of the equation corresponds to the point in the reference frame being transformed *to* (denoted with subscript 2), and the coordinates in the right-hand side corresponds to the same point but in the reference frame being transformed *from* (denoted with subscript 1). D denotes the scale factor while T and R denote the translation vector and rotation matrix, respectively, given by

$$
T = \begin{pmatrix} T_x \\ T_y \\ T_z \end{pmatrix}, \quad R = \begin{pmatrix} 0 & -R_z & R_y \\ R_z & 0 & -R_x \\ -R_y & R_x & 0 \end{pmatrix}.
$$

The dotted parameters of the coordinates ($\dot{x}$, $\dot{y}$, $\dot{z}$) and the Helmert parameters ($\dot{T}$, $\dot{D}$, $\dot{R}$) designate their respective first time derivatives, or sometimes called rates.

Furthermore, each pair of TRFs require a unique set of Helmert transformation parameters. As such, these should be provided in any application where a transformation between TRFs is necessary. Equation (2.1) also assumes that the positions of each point are valid at the same reference epoch, or else that they have been propagated to a common moment in time. For each pair of reference frames the transformation is only valid one-way, from one frame to the other. Transforming back to the original reference frame require the coordinate subscripts 1 and 2 to be switched, and for the transformation parameters to have their signs changed (Altamimi et al. 2017b).

To give a sense of magnitude of a typical Helmert similarity transform, the translation parameters are usually given in the unit millimeter, the unitless scale factor in parts-per-million (ppm) or parts-per-billion (ppb), the rotation parameters in milliarcseconds, and their respective time derivatives are given per year.

2.3 Estimation of the 7-Parameter Transformation

Each set of transformation parameters to transform coordinates between two reference frames are valid for every physical point in the frame. However, if considering just a single point at a time, in reality each point will likely require a slightly different set of parameters to transform the coordinates. Because of this a (weighted) least-squares approach is usually used to estimate the transformation parameters and their respective errors for each set of reference frames.

To estimate the seven parameter transformation the first step is to find reference points in a network whose coordinates are known precisely both prior to and after the transformation. Using the positions of these points in both reference frames in conjunction with the first row of Equation (2.1), an equation system can be set up suitable for a least-squares solution. To determine all seven parameters, and since each reference point yields three equations due to its x, y, and z coordinates, it should be noted that *at least* three reference points common to both reference frames are necessary, or else the system will be rank-deficient.

Thus, three equations can be constructed using the x, y, and z coordinates for a station, following Equation (2.1). Moving the first term of coordinates in the right-hand side to the left-hand side, each set of station positions yield the following system of three equations

$$\begin{cases} x_2 - x_1 = T_x + D \cdot x_1 + R_y \cdot z_1 - R_z \cdot y_1 \,, \\ y_2 - y_1 = T_y + D \cdot y_1 - R_x \cdot z_1 - R_z \cdot x_1 \,, \\ z_2 - z_1 = T_z + D \cdot z_1 + R_x \cdot y_1 - R_y \cdot x_1 \,. \end{cases} \tag{2.2}$$

After stacking the system of Equations (2.2) for every station i in the network common to both TRFs, the fully stacked equation system can be used to solve for the seven Helmert parameters. Perhaps more easily digestible (and more easily applicable to any computational software) is the matrix form of the equation system (Petit and Luzum 2010)

$$b = \begin{pmatrix} \vdots \\ x_2^i - x_1^i \\ y_2^i - y_1^i \\ z_2^i - z_1^i \\ \vdots \end{pmatrix} \,, \quad A = \begin{pmatrix} \vdots & \vdots & \vdots & \vdots & \vdots & \vdots & \vdots \\ 1 & 0 & 0 & x_1^i & 0 & z_1^i & -y_1^i \\ 0 & 1 & 0 & y_1^i & -z_1^i & 0 & x_1^i \\ 0 & 0 & 1 & z_1^i & y_1^i & -x_1^i & 0 \\ \vdots & \vdots & \vdots & \vdots & \vdots & \vdots & \vdots \end{pmatrix} \,,$$

where b is the so-called vector of observations, and A is the design matrix whose seven columns correspond to each of the seven transformation parameters, three translation, one scale factor, and three rotation angles. When solving this system of equations the ordinary least-squares method can be used, with the risk of the solution being sensitive to outliers. Weighted least-squares could be applied instead if, for instance, the formal errors of the station positions in the transformed frame are known.

2.4 Realisation of the ITRS - The ITRF

The reference system that has been formally adopted by the geodetic community is the ITRS. The ITRS has been thoroughly defined by the International Earth Rotation and Reference System Service (IERS) in Petit and Luzum (2010). The IERS is also in charge of the realisations of a terrestrial and a celestial reference system, the ITRF and the ICRF, respectively. Because of new and improved space-geodetic equipment, and newer and more accurate models for various phenomena affecting said equipment, the IERS also works continuously by maintaining the ITRF, which is updated every few years. The fully detailed descriptions and explanations of each iteration of the ITRF is available through their respective authors, with the most recent iteration being the ITRF2020 (Altamimi et al. 2022).

To be able to realise the ITRF, the ITRF team receives contributions from the four major space-geodetic techniques through their respective services, the International GNSS Service (IGS), the International VLBI Service for Geodesy & Astronomy (IVS, see Nothnagel et al. 2017), the International Laser Ranging Service (ILRS), and the International DORIS Service (IDS). Because all four techniques are being used, the network of stations is distributed all over the globe. The network of sites used to establish the ITRF2020 can be seen in Figure 2.3. It should be noted that the distribution of sites is inhomogeneous between the Northern and Southern Hemispheres for some of the space-geodetic techniques.

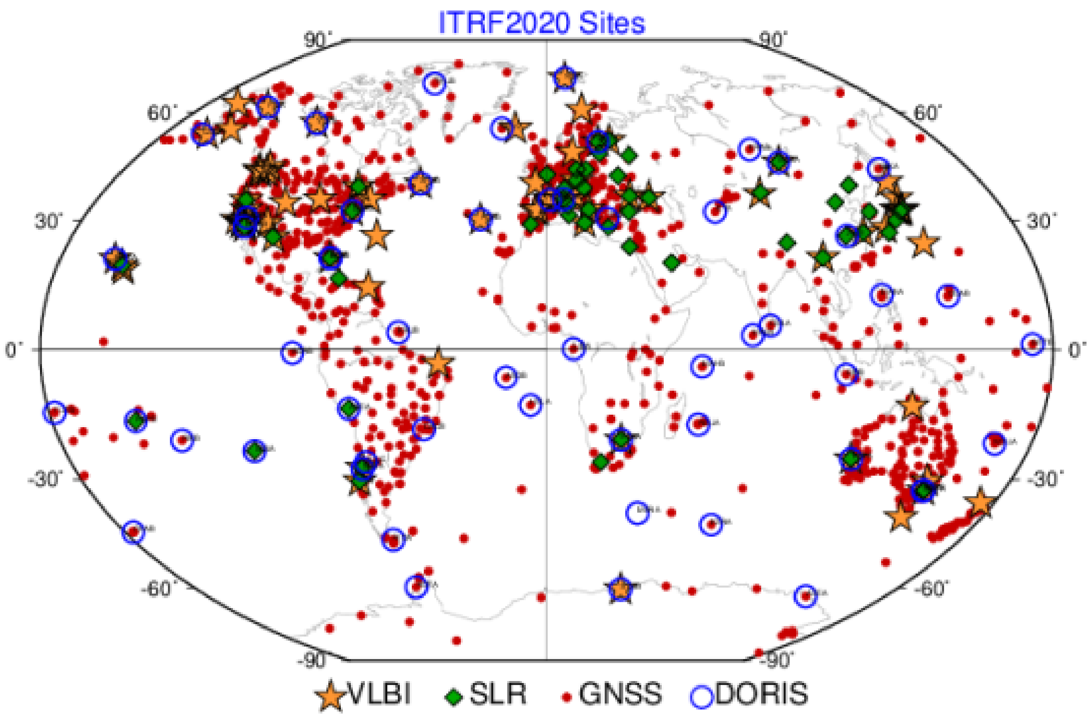

Figure 2.3: Map of all technique-specific ITRF2020 network sites. Sites containing equipment from two or more space-geodetic techniques are called co-location sites and are essential in realising the ITRF2020. (Credit: `https://itrf.ign.fr/en/solutions/itrf2020`)

Table 2.1: The ITRF2020 contributions from each of the four major space-geodetic techniques, during their respective time spans.

Technique	Time span	# of solutions	# of sites
DORIS	1993.00-2021.00	1456 weekly	87
GNSS	1994.00-2021.00	9861 daily	1159
SLR	1983.00-1993.00	243 fortnightly	100
	1993.00-2021.00	1460 weekly	
VLBI	1980.00-2021.00	6178 session-wise	117

Each of the space-geodetic techniques have their own set of advantages, disadvantages, and challenges. The techniques are also at varying stages of development, they are unevenly distributed around the globe, some have been operating for longer periods of time than others, and the regularity of measurements or sessions are different. For instance the satellite-based techniques (DORIS, GNSS and SLR) are very sensitive to changes in the Earth's centre-of-mass since that is also the point around which the satellites orbit, but VLBI is not.

By having the strengths of one technique compensate for the weaknesses of another, it allows the realisation of the ITRF to be more accurately defined. This is made possible by having ground stations of at least two space-geodetic techniques co-located close to each other at different sites around the globe, and thus connecting the reference points of each local station using local tie vectors (Petit and Luzum 2010; Altamimi et al. 2016). However, as proposed by Poyard et al. (2020), accurate surveying of the local tie vectors is important to make this method reliable.

2.4.1 ITRF Combination of Four Solutions

When realising the ITRF, the first step is to establish four long-term frames from the solutions of each technique (Altamimi et al. 2016). These four long-term frames are then combined through the use of co-location sites which are essential to the ITRF computation. Briefly discussed in Section 2.4, these are sites that contain instruments for two or more space-geodetic techniques. These reference points, or instruments, are then connected using reference vectors that have been precisely surveyed locally. Looking at Figure 2.3 and Table 2.1 it becomes apparent that the GNSS stations are by far the greatest in number and contribute to many co-location sites (Altamimi et al. 2016). An example of a co-location site is the Onsala Space Observatory seen in Figure 2.4, with radio telescopes and GNSS receivers. However, there is no equipment for DORIS as that would require emittance of waves that might disturb other instruments.

Figure 2.4: Radio telescopes at the Onsala Space Observatory. GNSS receivers are located nearby making this a co-location site. (Original image by: Onsala Space Observatory/Anna-Lena Lundqvist)

The actual ITRF product is essentially a list, or a catalogue, of precise positions for each station in the IERS network. This data is provided on a per-technique basis for the corresponding technique network. For instance as a VLBI user this means that access is granted to the positions and velocities of each VLBI station in the network, as well as other parameters such as the Earth Orientation Parameters (EOPs) to link the current model of the ITRF to the current model of the International Celestial Reference Frame (ICRF) (Charlot et al. 2020). Newer iterations of the ITRF also include more parameters to correct for station displacements, such as coefficients to correct for a post-seismic deformation model or seasonal signals which will be discussed later (Altamimi et al. 2022).

2.4.2 Consistency Between ITRF Iterations

The realisation of the ITRF is updated every few years, with the first realisation being called ITRF92 and the latest ITRF2020. The ITRF has to be updated to keep up with motion of the Earth's crust, but also because of things such as newer equipment and models that can enhance the products. Obviously using the latest solution of the ITRF is desirable, but it might be just as important to have the ability to transform coordinates between newer and older iterations. With each new iteration of the ITRF comes transformation parameters to transform coordinates between iterations. The Helmert transformation parameters to transform between past ITRFs are available at:

`https://itrf.ign.fr/en/solutions/transformations`.

Ideally the Helmert parameters between one iteration of the ITRF and another should all be equal to zero, or at least very close to it. That is because each new iteration of the ITRF is supposed to be an updated realisation of the previous ITRF. The constraint is added to minimize the difference between every iteration of the ITRF. To achieve this alignment between solutions, further constraints can be added such as the minimum constraints of No-Net-Translations (NNT) of points, and No-Net-Rotation (NNR) of the orientation (Soffel and Langhans 2013). For instance as defined by Altamimi et al. (2016), the origin of the ITRF2014 was defined so that there were zero translation parameters between the ITRF2014 and the ILRS SLR solution (NNT constraint), and a core network of stations were used to define zero rotation between the ITRF2014 and ITRF2008 orientations (NNR constraint).

Another important aspect that must be considered is that each realisation of the ITRF is defined at a reference epoch, t_0. For instance the reference epochs of the ITRF2014 and ITRF2020 are 2010.00 and 2015.00, respectively (Altamimi et al. 2016; Altamimi et al. 2022). However, because each iteration of the ITRF also contains estimates of the linear velocities of each station, it is possible to propagate the position of a station over time. At an epoch t, this propagated position becomes

$$X(t) = X(t_0) + \dot{X}(t - t_0)\,, \tag{2.3}$$

where the two terms X and $\dot{X}$ correspond to the available ITRF positions and linear velocity in the x-, y-, or z-direction. This allows the user to get a good estimate of the position of a station at another valid epoch.

2.4.3 Discontinuities and Kinematic Models

Simply linearly propagating the position of a station becomes an issue when said station has discontinuities in its position. Such a discontinuity could be due to reparation of an antenna, or the station being offline for a period of time, or similar. However, replacement of equipment would usually be handled as a new station entirely, and otherwise the ITRF includes a set of position and velocities for a station valid during different periods of time.

There are also other displacements of stations that are nonlinear in nature, for instance, a post-seismic deformation (PSD). When a station is hit by an earthquake, its motion following the event can be modelled using logarithmic and/or exponential terms. The sites affected by such events are limited, but it has to be accounted for nonetheless. The ITRF2014 introduced a PSD model to correct for these displacements, which is also used for later iterations of the ITRF (Altamimi et al. 2016). These corrections should be applied when propagating the position of an affected station to *any epoch after the earthquake*. It should be noted that the PSD models are fitted to follow the post-seismic trajectories of GNSS stations which Altamimi et al. (2017a) have proved fit the time series of co-located equipment very well.

The next iteration, the ITRF2020, also introduced correction terms for annual and semi-annual signals affecting station positions (Altamimi et al. 2022). These are estimations of cosine and sine terms at different frequencies. Similarly to the PSD correction terms, these seasonal terms are applied to the propagated station positions to correct for seasonal variations in positions. Also introduced by Altamimi et al. (2022) was the new kinematic model to express the station position of an affected station. At epoch t, expressed as decimal year, the position is given by

$$X(t) = X(t_0) + \dot{X}(t - t_0) + \delta X_{PSD}(t) + \delta X_f(t)\,, \tag{2.4}$$

where the first two terms correspond to the propagated position from its reference epoch t_0, similar to Equation (2.3). The third term δX_{PSD} corresponds to the total sum of PSD corrections, if such terms are applicable. Likewise, the last term δX_f is the sum of sinusoidal correction terms for seasonal signals, also only for stations where applicable.

To compute the total sum of PSD corrections for the ITRF2014 and later, the user should use all of the provided logarithmic and/or exponential coefficients to compute each of the components as

$$\delta L(t) = \sum_{i=1}^{n^l} A_i^l \log\left(1 + \frac{t - t_i^l}{\tau_i^l}\right) + \sum_{i=1}^{n^e} A_i^e \left(1 - e^{-\frac{t - t_i^e}{\tau_i^e}}\right)\,, \tag{2.5}$$

where A_i are the amplitudes, t_i the earthquake times, and τ_i the relaxation times of the ith terms. This goes for both the n logarithmic and exponential terms, each denoted by the superscript l or e, respectively. In practice there could be only logarithmic terms to best model the trajectory of a station, or only exponential terms, or both.

For the ITRF2020, and presumably also later iterations, the final term to correct for the seasonal signals should be computed in a similar fashion. As formulated by Altamimi et al. (2022), the sum of the sine and cosine terms can be written by

$$\delta X_f(t) = \sum_{i=1}^{2} \left[\begin{pmatrix} a_x^i \\ a_y^i \\ a_z^i \end{pmatrix} \cos(2i\pi t) + \begin{pmatrix} b_x^i \\ b_y^i \\ b_z^i \end{pmatrix} \sin(2i\pi t) \right] , \tag{2.6}$$

where the six a and b terms should be available for both the annual and semi-annual frequencies for all stations with sufficient time spans. As a final reminder, the fourth seasonal term δX_f computed in Equation (2.6) is not part of the ITRF2014 solution, only $\delta L(t)$ computed in Equation (2.5).

2.4.4 The IVS Contribution to the ITRF

One of the most significant contributions of the IVS to the ITRF long-term frames are the scales and scale rates. Historically the ITRF scale has been selected in such a way that there is zero scale and scale rate between the ITRF solution and the average of the VLBI and SLR scales and scale rates. Thus the contributions from the IVS, as well as the ILRS, have been essential when realising the scale of the ITRF.

Due to how the VLBI technique works the IVS provide solutions on a session-wise basis. The entire IVS network of stations does not participate in every session, in practice there can be as few as 2-3 stations, or upwards of 20 stations. The IVS coordinates both 24-hour sessions several times per week using a larger subset of stations, as well as daily 1-hour intensive sessions with fewer stations to determine universal time UT1 (Behrend 2013). Since 1979, and using over 150 different stations spread out over that time period, the VLBI technique has performed observations during thousands of sessions to determine EOPs, TRFs, and CRFs.

Since these sessions are performed as international collaborations, it is only fitting that each session is also processed by a number of individual Analysis Centers (ACs). The individual solutions are then combined before the IVS submits its combined solution to Altamimi et al. Figure 2.5 illustrates the IVS data flow from session-wise data to the final products.

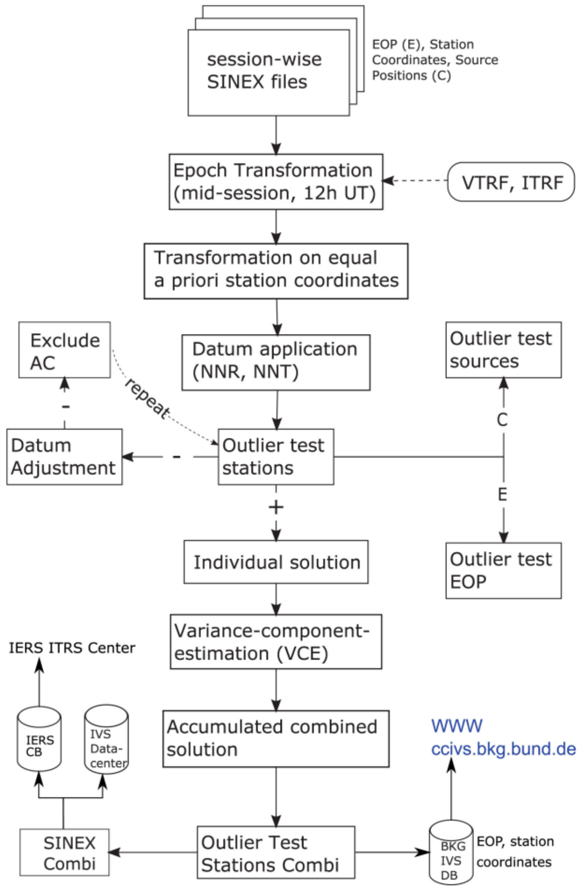

Figure 2.5: An overview of the IVS data flow, from session-wise solutions all the way to the IVS combined solution and EOP products. (Credit: Bachmann et al. 2017, p. 636)

It should be noted that out of eleven different individual ACs which submitted a solution to the IVS, seven different software packages are used to estimate the global solutions of TRFs. This diversity is considered a strength by the IVS when the individual solutions are combined into the IVS combined solution (Hellmers et al. 2022).

2.4.5 The SINEX Format and Identifying Common Stations

The IERS and the geodetic community uses a standard file format called the SINEX (Solution INdependent EXchange) format. Such a standard format is necessary as a way of transferring solutions between various analysis centers, groups, and applications. The ITRF is essentially provided by the IERS as a set of such SINEX files. This section will contain a brief description regarding the essentials of identifying common physical points between TRFs in this format. A more in-depth and detailed description of the SINEX format can be found at:

`https://www.iers.org/IERS/EN/Organization/AnalysisCoordinator/SinexFormat/sinex.html`.

When an AC has analysed a VLBI session, the solution is presented as a SINEX file containing all parameters necessary to define a TRF, and EOPs. The comparison of two TRFs, or two SINEX files, becomes a matter of identifying all stations common to both TRFs that exist in both files. The conventions for naming each VLBI station is based on the IVS naming conventions[1].

While this might seem like a trivial issue at first, in practice each VLBI station has been designated with multiple identifiers. There also appears to be no clear standard as to which identifier should be used in what scenario, but rather it is up to the user to select which one(s) to work with. With that said, there might be multiple designations used when referring to the same stations during later parts of this thesis, which might seem confusing and inconsistent when not familiar with the syntax. This is illustrated with an example, Table 2.2 contains the identifiers for the twin telescopes in Onsala, Sweden (seen in Figure 2.4).

Table 2.2: Example of IVS identifiers for the two 13-m telescopes at the Onsala Space Observatory.

IVS Code	IVS Station name	DOMES	CDP	Comments/description
Oe	ONSA13NE	10402S014	7636	Onsala 13-m antenna north-east
Ow	ONSA13SW	10402S015	7637	Onsala 13-m antenna south-west

The full explanation of each field is provided by the International VLBI Service for Geodesy & Astrometry (2022), but the main takeaways are the first 2-letter IVS codes that are commonly used during scheduling, and the 9-character DOMES[2] numbers used to identify not only stations but also site and technique-specific reference points. The 4-digit CDP numbers can also be useful when identifying stations, while the last field contains a simple description of the station.

2.5 Very Long Baseline Interferometry

Very long baseline interferometry (VLBI) is often considered to be a technique used for astronomy, but it is just as applicable for geodesy. Today this geodetic technique is essential to achieve the high level of accuracy in positioning that we often expect. Out of the four space-geodetic techniques it is the only one able to provide all EOPs, and thus the only technique to provide universal time and celestial pole movements. It also plays the important role of linking a TRF rotating with the Earth to a non-rotating celestial reference frame (CRF) in space, and thus maintaining the stability of EOPs (Schuh and Behrend 2012).

[1]The IVS list of network stations can be found at `https://ivscc.gsfc.nasa.gov/products-data/index.html`, under *Network station codes, CDP numbers, and DOMES numbers.*

[2]For further information about DOMES numbers see `https://itrf.ign.fr/en/network/domes/description`.

2.5.1 Basic Concept and Geometry

The idea behind VLBI is to have a network of several radio telescopes spread around the world, where multiple radio telescopes can observe the same distant extragalactic radio sources in space. Because the sources are so far away, the radio waves arrive on Earth as plane wavefronts (Schuh and Böhm 2013). These are recorded at each telescope along with a very precise timestamp obtained from stable atomic clocks, such as hydrogen masers. The recorded signals, corresponding to the arrival times, from each radio telescope are then sent to a so-called correlator where the signals are combined and superimposed. The VLBI time difference between each pair of telescopes that have observed the same source can then be determined (Robertson 1991). The concept is visualised in Figure 2.6, where plane wavefronts arrive at each radio telescope (1 and 2) with a time delay τ, where the signals are digitized and sent to a correlator for analysis.

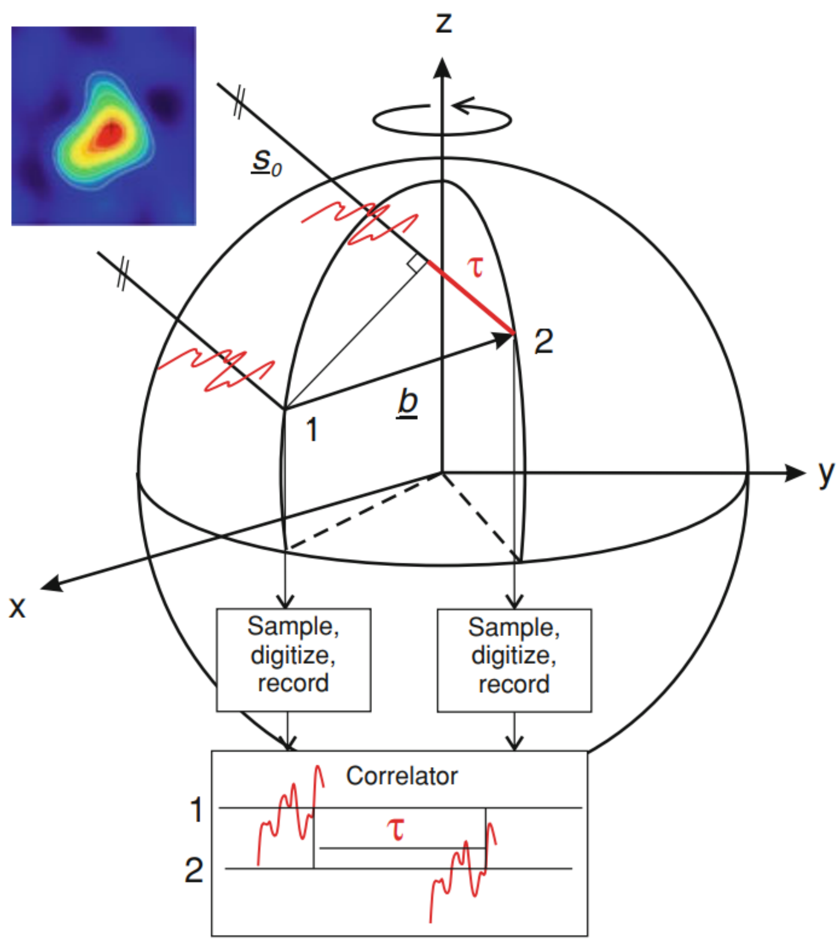

Figure 2.6: Schematic of the VLBI technique. Plane wavefronts from a distant radio source arrive at each telescope with a time delay τ, determined by combining both signals. (Credit: Schuh and Böhm 2013, p. 340).

The goal is to create baselines (denoted $\underline{b}$ in Figure 2.6) between every significant combination of two stations in the network. The baselines are what allow the VLBI technique to achieve such high accuracy. That is because the angular resolution of a telescope depends on the observing frequency and its diameter, thus by using interferometry to link telescopes it allows the baseline between each pair to act as a single very large radio telescope. While the physical size of a single antenna is limited in size at the order of meters, a single baseline can be as long as thousands of kilometers.

The general flow of operations for the VLBI technique can be seen in Figure 2.7, showing the many different corrections that have to be made to each measurement during analysis. For instance things such as instrumental calibrations, atmospheric effects, and deformations amongst others all have to be accounted for. Just like with all other techniques, the accuracy at which these corrections are made will directly impact the performance of VLBI. Thus, some error sources will be discussed briefly.

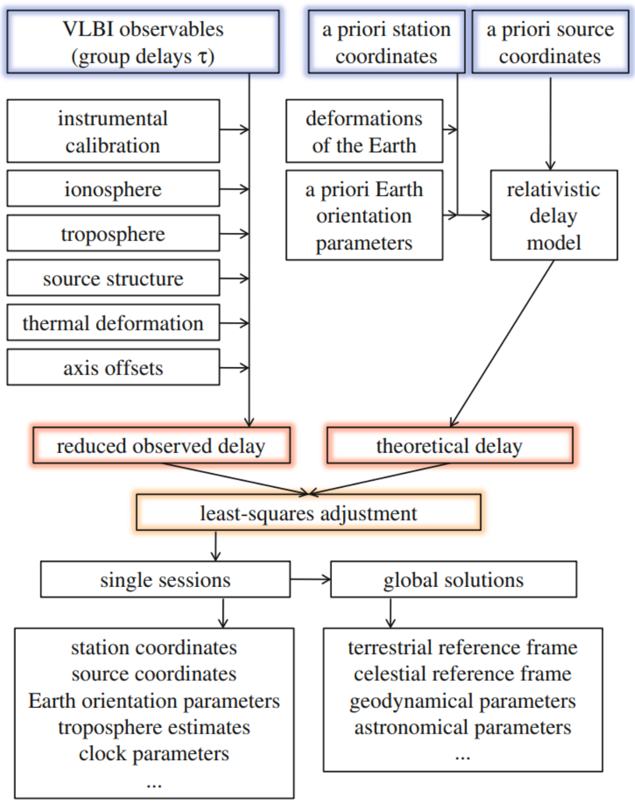

Figure 2.7: Flow chart of the VLBI data analysis, and of all corrections that have to be made. (Credit: Schuh and Böhm 2013, p. 347)

2.5.2 Possible Error Sources to Consider

The observed radio waves are of course sensitive to things that affect every electromagnetic wave. For instance, the atmosphere has significant impact, and any atmospheric and tropospheric delays have to be accounted for, meteorological data and modelling has to be up-to-date, and relativistic and other corrections have to be made (Nilsson and Haas 2010). But also phenomena that physically affect the actual telescope have to be considered. The telescope might be located in a region where the antenna gets deformed by extreme temperature differences or atmospheric pressure and hydrology loading, or continental drift might be causing it to move (Schuh and Böhm 2013).

Furthermore, as is inherent to all antennas, accuracy can be greatly affected by how accurately the reference point (antenna phase center) is determined, which is usually an immaterial point at the intersection of the antenna axis (Heinkelmann 2013). As suggested by Nilsson et al. (2017), that implies that axis offset have to be accurately determined and consistently applied during data analysis. Considering co-location sites for the ITRF, as discussed in Section 2.4, this might be of even more importance to accurately determine local tie vectors between stations. Lastly, there are also other practical things that might negatively affect the VLBI measurements if not accounted for, for instance maintenance of the antenna, connecting cables, and other instruments have to be considered.

2.5.3 Scheduling, Sessions and Networks

Performing measurements using VLBI is a bit more complex than simply turning on a receiver. By design it requires the inclusion of VLBI stations simultaneously observing the same radio sources while being spread around the globe. These observation sessions are scheduled far in advance by the IVS, and this separates the VLBI technique from the other space-geodetic techniques in the sense that it cannot perform measurements on the same regular basis. Instead the measurements are performed on a session-wise basis, but the sessions are scheduled for multiple times a week and using similar networks of stations. In the context of realising a TRF, the session-wise basis means that despite a session spanning 24-hours, all observations have to be approximated to a single moment in time, usually in the middle of a session.

Each VLBI session performs observations with a set of stations that create a network. Unfortunately, it is in practice impossible for sessions to use precisely the same network of stations every single time. There might be maintenance of equipment, the radio telescopes on a site might be booked for other purposes, a hard drive might fail in the middle of an observation, and so on. The VLBI stations are also inhomogeneously distributed around the globe, as seen in Figure 2.3. This can be a limitation during a VLBI session since at least two telescopes have to be able to observe the same radio source simultaneously.

In recent years, some sites have also adopted and begun operation using so-called twin radio telescopes. An example being the Onsala Space Observatory seen previously in Figure 2.4, where the telescopes can work in conjunction or observe different sources during a session. Note that these telescopes also create a very short baseline between each other, one which may be excluded in the analysis process.

2.6 Restating the Problem

Before continuing on, this is an appropriate time to restate the problem of this project. During preparation of the ITRF2020, an unexpected behaviour with VLBI scale time series from the IVS combined solution presented itself. Because the long-term solution of the IVS and ILRS solution frames would be the basis for the scale of the ITRF2020, the scale was computed between the preliminary ITRF2020 and the previous ITRF2014. However, despite the IVS combined solution covering the entire time period of 1979 through 2021, it was noted that the scale factor was behaving unexpectedly during the last few years. This phenomena can be seen in Figure 2.8.

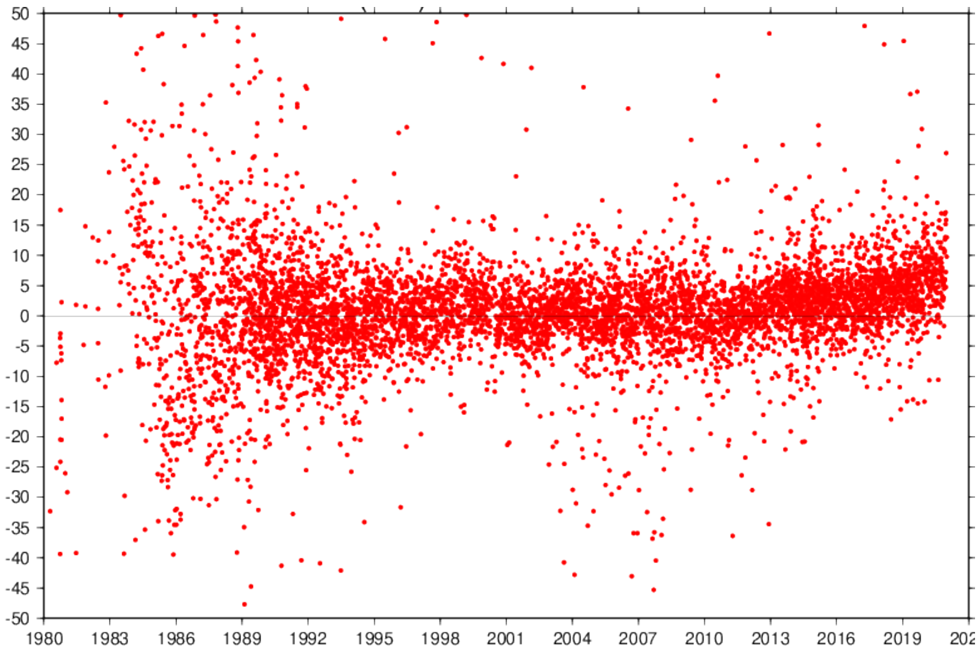

Figure 2.8: The ITRF2020 VLBI scale time series expressed in mm. Note the behaviour beginning around late 2013, where the scale factor appears to show some drift. (From: `https://itrf.ign.fr/en/solutions/ITRF2020`)

Because of this, Altamimi et al. (2022) did not use the entire time series up until 2021.00 to determine the ITRF2020 scale. Instead only selected VLBI sessions up to epoch 2013.75 were used for the final product. Ideally the entire time series of data should be used, especially since VLBI has been contributing with data for the longest time out of the four space-geodetic techniques (see Table 2.1). For some context as to how substantial a drift in the scale might be, at the equator a scale factor of ≈ 0.15 ppb translates to ≈ 1 mm.

Thus, this project set out to attempt to find some connection between the scale and various properties of the VLBI network. The following chapters will present what analysis software packages were used and how the investigations were conducted. Studies include adding artificial motion to stations, excluding stations from global solutions, and observing the VLBI network volumes and distributions.

3

Analysis Software

This chapter describes the software packages and tools that were used and developed during this project. The ITRF2014 was used as the frame of reference for comparison with other different solutions throughout the entirety of this project. That is because the ITRF2014 was the latest freely available iteration of the ITRS when the project started. The products of the ITRF2014, its full description, and files are available from the IERS at:

`https://itrf.ign.fr/en/solutions/ITRF2014`.

It should be noted that since the start of the project the ITRF2020 has been published and is available but unfortunately this was too late into the project to justify such major changes. The ITRF2020 files are available at:

`https://itrf.ign.fr/en/solutions/ITRF2020`.

3.1 Other Solution TRFs for Comparison

With the ITRF2014 determined as the TRF of comparison, the other TRFs are realised by every VLBI 24h-session and its corresponding solution(s). Each individual solution of station position estimates and EOPs realises a TRF. This derived TRF is in turn valid for the reference epoch of the corresponding VLBI session, with both station positions and velocities. It then becomes a matter of identifying the common points, or common stations, between this reference frame and the ITRF2014 for comparison.

Thanks to the contribution and help from Onsala Space Observatory, and Lantmäteriet, 6932 session solutions were made available to use during this project. That included data spanning the entire lifetime of VLBI, all the way from August of 1979 through July of 2021. Thus the OSO solution became a major part of this project, and became the individual AC solution that various studies on the scale factor were performed and based upon. The different OSO solution TRFs to be compared to the ITRF2014 included solutions where specific stations had been excluded entirely from the solution, or where specific stations had their position and velocity estimates artificially disturbed.

In particular the seven parameters for the Helmert transformation have been estimated between the ITRF2014 and OSO solutions for the ITRF2020. This was done following the procedure as described in Section 2.3. However, instead of estimating the seven Helmert parameters and their respective errors using the ordinary least-squares method it was deemed appropriate to perform weighted least-squares instead. The weights that were used corresponded to the inverted variance of each estimated coordinate in the so-called OSO solution TRF. That is to say that the diagonal of the weight matrix consisted of the inverted and squared formal error of these coordinates. In matrix form the diagonal vector w was expressed as

$$w = \begin{pmatrix} \vdots \\ (\sigma^i_{x1})^{-2} \\ \\ (\sigma^i_{y1})^{-2} \\ \\ (\sigma^i_{z1})^{-2} \\ \vdots \end{pmatrix},$$

where σ^i denotes the formal error of the x_1, y_1, and z_1 coordinate estimates for station i.

3.2 Using the ASCOT Software Package

ASCOT (Analysis, Scheduling and Combination Toolbox, see Artz et al. 2016) is a VLBI software package originally created by the VLBI group of the Institute of Geodesy and Geoinformation of the University of Bonn (IGG). It is currently maintained and further developed by the group for Space Geodesy and Geodynamics at the OSO AC. The software is implemented in C++ and can perform both VLBI scheduling and geodetic data analysis. ASCOT was used by the OSO AC to compute its individual solutions for the IVS contribution to the ITRF2020. During this project ASCOT was used to reprocess the very same VLBI sessions that had been submitted to the IVS combination solution.

The software package is able to perform single-session VLBI data analysis to derive global solutions of TRFs. This functionality was used extensively during this project. ASCOT is organized so that it takes the input of a configuration file including a list of VLBI sessions to process one at a time. The configuration file allows the user to specify how to handle, or compute, each step in the solution process. Without going into unnecessary detail, it generally entails configuring what method(s) to use when handling each step of the VLBI data analysis (see Figure 2.7). For instance, that would be if any sources, stations or baselines should be excluded, what corrections to perform when available data is missing or ambiguous, and so on.

Due to the time constraint of this project, aiming at understanding the software from the ground up was not a feasible option. Instead the same configuration files and corresponding data files that were used for the ITRF2020 contribution were used and only slightly modified. Those files included things such as meteorological data, tropospheric models, a priori positions, etc. The ability to exclude any station(s) from the entire solution was also used, which will be discussed later.

3.3 Routines of the Scalestigator

A majority of the time spent during this project was spent developing a toolbox to be used to estimate the seven Helmert transformation parameters with reference to the ITRF2014, and the scale factor in particular. The toolbox was created using the software *MATLAB ver. R2021b*[1] and designed to work with the aforementioned SINEX files. By adhering to this file format it also means that adaption to any future, or earlier, iterations of the ITRF becomes a relatively straight-forward process.

3.3.1 Storing ITRF2014 Catalogues

While the SINEX format is well-documented, it was deemed unnecessary having to read multiple files during every operation. Instead a so-called catalogue was created, roughly inspired by a lookup table to reduce runtime. That way only a single .mat-file could be loaded once, instead of reading one file for station positions and velocities, another for station discontinuities, and yet another for PSD correction coefficients.

The first tool to be developed created a catalogue which contained the IVS portion of the ITRF2014. That included all 154 VLBI stations with their positions and linear velocities at the reference epoch 2010.00. 33 stations were also listed as having experienced some kind of discontinuity, and these have multiple positions and velocities that are internally identified as solution numbers (SOLN), each SOLN valid during a certain period of time. Thirteen of these stations had experienced some form of discontinuity and also included corresponding PSD coefficients to correct for the motion.

Using the positions and velocities of all ITRF2014 VLBI stations, it was then possible to compare it to other TRFs. These were the so-called solution TRFs by individual ACs, provided as SINEX files. The first step was to identify every station in the network that also appeared with corresponding positions and velocities in the ITRF2014. These were identified using both the DOMES and CDP numbers for each station, as described in Section 2.4.5. By ignoring sessions with none or less than three common stations, an equation system could later be constructed according to the system of Equations (2.2).

3.3.2 Propagating ITRF2014 Stations

The next tool to be developed was necessary for the comparison between a solution TRF and the ITRF2014. The station positions of each station in the ITRF2014 had to be propagated to the same reference epoch t as the considered VLBI session. For

[1] *MATLAB version 9.11.0.1873467 (R2021b) Update 3* 2021.

a majority of stations this propagation corresponded to regular linear motion from the ITRF2014 reference epoch $t_0 = 2010.00$ to the reference epoch of the other TRF t, as per Equation (2.3). Because the velocities are provided in the unit mm/yr, the conversion from a (modified) Julian date to decimal year was necessary, and was done by dividing by 365.25. For a station with multiple positions and velocities (because of some discontinuity), the position and linear velocity was selected from the corresponding SOLN valid at epoch t.

When a station had been affected by an earthquake, the PSD correction term computed using Equation (2.5) was added if any logarithmic and/or exponential terms were available for the station. This term required the station positions to be transformed from x, y, and z coordinates into local East, North, and Up components. The two coordinate systems are commonly denoted as XYZ and ENU, respectively, and the geometry can be seen in Figure 3.1. In such a case the GRS80 ellipsoid was used as reference, according to IERS conventions (Petit and Luzum 2010).

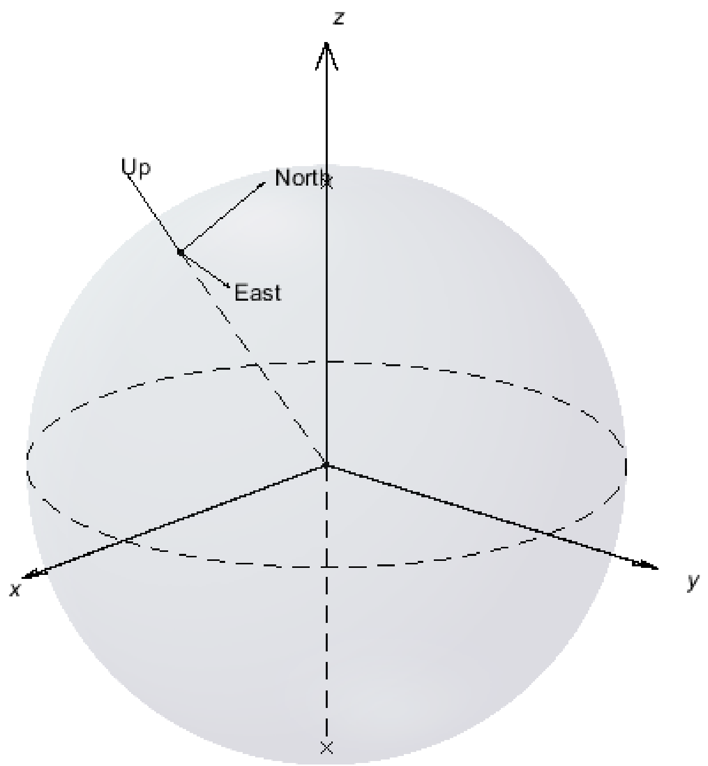

Figure 3.1: Local ENU coordinate system at some point on the Earth. The Up-component pointing radially away from the geocenter, the orthogonal North-component pointing towards the North Pole (or positive z-axis), and the East-component orthogonal to both.

The propagated position was then computed as per Equation (4.1), while ignoring the δX_f term which was not added until the ITRF2020. When compared to the IERS station positions, this propagation tool was able to reproduce the estimated positions of any station found in the ITRF2014, from the reference epoch of 2010.00 to any desired date. Thus, this tool was used during studies when comparing the TRF of a VLBI session with reference to the ITRF2014. The function of this tool was also extended to allow any artificial linear velocity to be added to a selected station, allowing for the simulation of mismodelled uplift.

3.3.3 Estimating Helmert Parameters Between Two SINEX Files

Another tool that was developed and used was the ability to estimate the seven Helmert parameters between any SINEX file and a given reference frame. This was done by having first identified all common VLBI stations of the solution TRF and the ITRF2014, then propagated each ITRF2014 to the corresponding reference epoch of the solution TRF, and then finally stacking the system of Equations (2.2).

Following the procedure described in Section 2.3, the tool then used a weighted least-square method to estimate the values and formal errors of the three translation parameters (T_x, T_y, T_z), the scale factor (D), and the three rotation parameters (R_x, R_y, R_z). The weights were used according to Section 3.1. That is to say that the formal error of the TRF x-position was used to compute the weight for the corresponding x-position equation, and so on.

3.3.4 Computing Network Volumes

Another tool was developed to store data regarding the network of each VLBI session. Of interest were the number of stations, but also each baseline and its corresponding length. In a network of n stations there are $\frac{n(n-1)}{2}$ unique combinations of two stations, each corresponding to a baseline. The length of each baseline corresponds to the distance between each pair of three-dimensional station positions.

The network volume of each station network was also computed using this tool. Here it is important to note that the computed network volume corresponded to the network of stations used to estimate the Helmert parameters. Because any stations not included in both the TRF and the ITRF2014 had been ignored, this network might contain fewer stations than the number participating in the VLBI observing session. To derive the network volume of a set of stations this tool made use of a Delaunay triangulation. This proved to be an efficient method of connecting all stations and computing the volume in three-dimensional space. The network volume of a session can be seen in Figure 3.2.

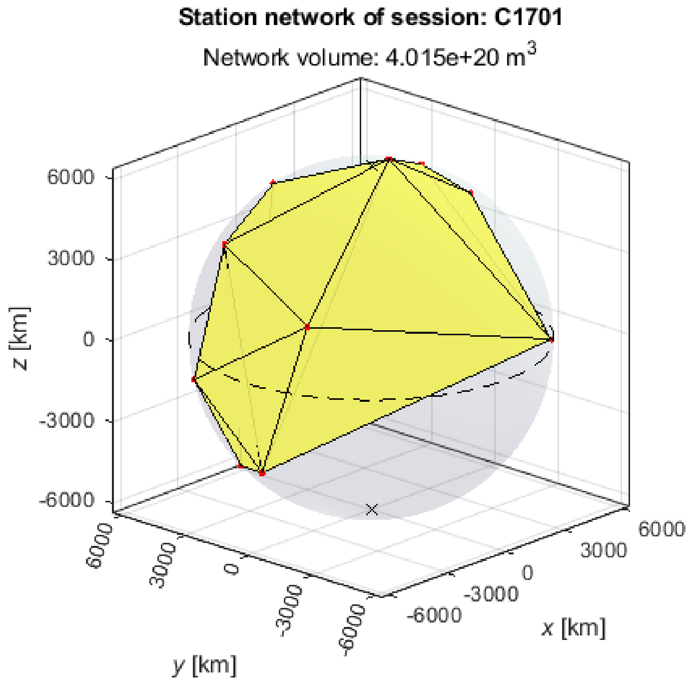

Figure 3.2: Visualisation of a Delaunay triangulation and corresponding station network volume of a VLBI session (session code C1701).

3.3.5 Additional Notes

As such, the development of a MATLAB toolbox was concluded. The toolbox allows for the comparison of global solution TRFs to the ITRF2014, through their respective set of SINEX files. The tools implemented are used to find all common reference points between two TRFs, propagate the comparison frame (the ITRF2014) to the reference epoch of the VLBI session SINEX file, and then estimate the seven Helmert transformation parameters between the two frames. The tools also compute and store information regarding the VLBI network used to estimate the Helmert parameters, including network volume, number of stations, and their approximate geographic coordinates (latitude, longitude, height). Before moving on to the applications of these tools, it should be noted that due to the very similar structure of the ITRF2020, the inclusion of the newly introduced semi-annual and annual corrections would be possible in the future.

4

Studying the Scale

This chapter explains how the different simulations and experiments were used to study the scale behaviour. It goes into more detail about how the previously discussed software packages were used to perform post-processing on different VLBI TRF solutions, but also how the reprocessing of new solutions was performed.

It should be noted that the causes that were investigated, and the studies that were conducted, were selected as the project was progressing. Because the scale behaviour was still under investigation, there was no previous work or literature to proceed from. Thus, different causes were investigated as new ideas arose.

4.1 Simulating Mismodeling of Uplift

The first approach of tackling the problem with the scale drift was to intentionally disturb the position of a single station in a VLBI session. The idea was to see how the scale would behave if just a single station would have its position and velocity parameters mismodelled. The disruption was added to simulate erroneous uplift of the station, the term uplift referring to the vertical motion (Up-component in Figure 3.1) of a station. For some context, uplift could be caused by post-glacial rebound that is often tracked and modelled using a local GNSS network, very common on the Fennoscandian Peninsula (Vestøl et al. 2019). Because the corrections to uplift very often are modelled from regular measurements of GNSS, these models are susceptible to errors just like any others. This study was performed to get an idea of how the scale would behave if that was the case.

The artificial uplift error was added to simulate the same scale drift behaviour seen during the time period 2013.75 to 2021.00, but during the time period before that. That is to say that the *bad* scale drift occurs in the *bad* time period of 2013.75 to 2021.00, while the *good* and expected scale drift occurs during the *good* time period *before* 2013.75. So the goal was to add uplift to simulate the *bad* scale drift rate during the *good* time period prior to 2013.75. This uplift was added to one station at a time by further adding to the propagated positions of the station in the ITRF2014, adjusting Equation (2.4) to

$$X(t) = X(t_0) + \dot{X}(t - t_0) + \delta X_{PSD}(t) + U(t - t_0), \tag{4.1}$$

where U corresponds to the artificially added uplift. Note that Equation (4.1) has dropped the δX_f term correction to seasonal signals since those were not added until the ITRF2020. The uplift was transformed from local ENU coordinates to XYZ, the geometry of which can be seen in Figure 3.1.

Due to the time limitation of this project, only a few stations were selected to have artificial uplift added for this experiment. The first station to be selected was the station in Ny-Ålesund, Svalbard, Norway. In the past few years this station has seen some change in the station position motion, with larger scatter and irregular position as seen in Figure 4.1.

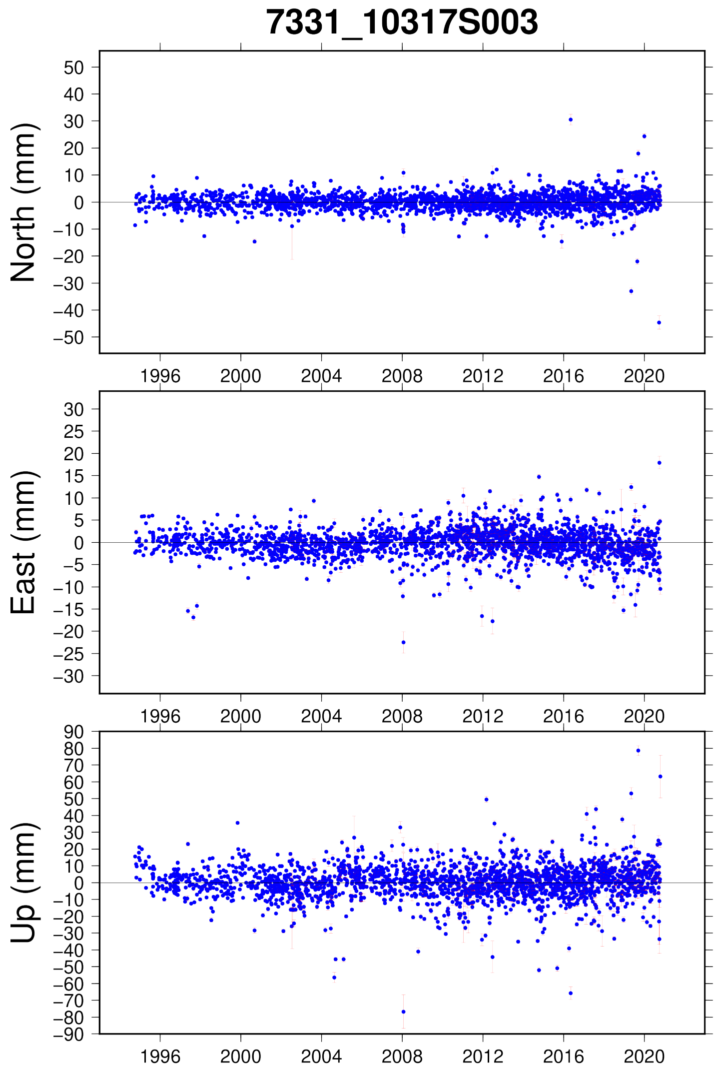

Figure 4.1: Position time series residuals with reference to ITRF2020 for the station in Ny-Ålesund, Svalbard (CDP number 7331, DOMES number 10317S003). This station was selected due to its larger scatter and irregular position in the past few years. (From: `https://itrf.ign.fr/en/timeseries`)

The station in Ny-Ålesund is the northernmost VLBI station in the network. Because it was also suspected that the global distribution of stations could have an impact on the scale, two additional stations were selected based on them being located far away from Svalbard. The second station was located at a southern latitude in Hobart, Australia, and the third station in Kokee Park Geophysical Observatory, Hawaii, which lies closer to the Equator. The idea for this was that a relatively clustered network on the globe would pull the TRF in that direction. Hence why removing the station in Ny-Ålesund, one of the few northern stations, was suspected to also remove the pull towards the north. The IVS identifiers of all three stations are found in Table 4.1.

Table 4.1: Identifiers for the three stations that were selected for the artificial uplift experiment.

IVS Code	IVS Station name	DOMES	CDP	Comments/description
Ny	NYALES20	10317S003	7331	Ny Alesund, Svalbard, Norway
Kk	KOKEE	40424S007	7298	Kokee Park, Kauai, HI, USA
Ho	HOBART26	50116S002	7242	Hobart, Tasmania, Australia

Finally, with the three stations selected as seen in Figure 4.2, a lower limit of epoch 1995.00 was also imposed on the *good* time period. Reason being because that was around the same time that all of the three telescopes started being used, and because the scale during the earlier years of VLBI could be considered relatively unstable. In fact, the selected VLBI sessions used for the ITRF2020 scale were very few prior to 1995.00 (Altamimi et al. 2022).

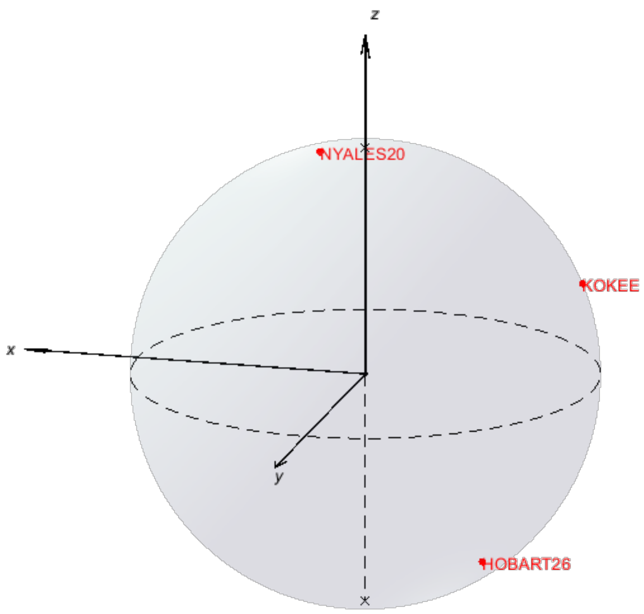

Figure 4.2: The three stations selected for the simulated uplift study. They were each selected at different latitudes of the VLBI network, one far north, one far south, and one closer to the Equator.

4.2 Reprocessing Solution TRFs with Exclusions

Another issue that was suspected to have an impact on the scale factors was the purely technical aspects of a VLBI station network. These aspects could be that a new station has been recently added to the network, that some station has required maintenance more frequently than others, or other similar issues. This idea came to be because of the fact that not all VLBI stations in a network are identical. Some may be equipped with different antennas, storage devices, atomic clocks, and the same goes for all other hardware (and software). To determine if such aspects could indeed affect the TRF scale of a solution, a study was conducted where selected stations were excluded from a solution entirely.

For this experiment, the OSO solution was reprocessed using ASCOT (see Section 3.2) a total of five times: 1) a solution with all sessions and stations as a benchmark, 2) three solutions where three different stations were excluded from the entire solution, one at a time, 3) one solution where every session containing a specific network was excluded. Instead of having to reprocess the entire 40+ years of data multiple times, in the interest of time only sessions during all of 2013 through all of 2020 were reprocessed, corresponding to the epochs 2013.00 to 2021.00. Two of the three stations that were excluded individually were selected on the basis that they had been operating consistently during the *bad* time period, but while encountering some sort of technical difficulties. The selection of the third station was based on mismodeling, as discussed in Section 4.1.

4.2.1 Station Technical Aspects

The first station to be excluded was the relatively new (added in 2014) VLBI station in Sejong, South Korea. During the correlation stage this station has commonly dropped several S-band channels leading to sub-ambiguities and noisy data. The station operators have also reported data storage issues and loss of data.

The second station that had experienced technical issues was the 40-m radio telescope at Yebes, Spain. This station was selected because its position had experienced a discontinuity in the ITRF2014 due to the sub-reflector of the antenna being moved. Before the end of 2011 the sub-reflector was moved to counteract gravitational deformation, but later it has been held fixed in place during geodetic VLBI experiments. A model has been implemented to mimic the effects of this sub-reflector. To study the effects of such a discontinuity, the station was excluded in one solution.

Referring back to Section 4.1, the third reprocessed solution to have a single station excluded had the station selected with the same ideas about network volume and distribution in mind. That was the same radio telescope in Ny-Ålesund, the idea being to exclude a large part of the Northern Hemisphere from the network volume.

Table 4.2 contains the identifiers for each of the three stations that were excluded. The IVS station names were used to exclude them using the ASCOT software.

Table 4.2: Selected single stations that were excluded from each reprocessed ASCOT solution one at a time, identified using the 8-character station names.

IVS Code	IVS Station name	DOMES	CDP	Comments/description
Ny	NYALES20	10317S003	7331	Ny Alesund, Svalbard, Norway
Kv	SEJONG	23907S001	7368	Sejong (KVG), South Korea
Ys	YEBES40M	13420S002	7386	40-m antenna at Yebes, Spain

4.2.2 Network Homogeneity

The VLBI network has evolved over the past few years. Some developments include a transition to the VLBI Global Observing System (VGOS, formerly VLBI2010), and also the introduction of additional sessions using the entire Very Long Baseline Array (VLBA, see Johnson et al. 2019). The VLBA was taken into consideration because we thought the increase of sessions based on only northern baselines would have an impact on the scale. Similarly, the transition to VGOS also added to this problem of homogeneity between northern and southern baselines, and stations observing during different session types, but the transition to VGOS was not studied in detail here.

Every session using only the VLBA network during observations were excluded in the fifth reprocessed solution. In reality the VLBA is not a single VLBI station like the internal identifier suggests but a network of ten stations located in the United States. The network of one such excluded VLBA session can be seen in Figure 4.3.

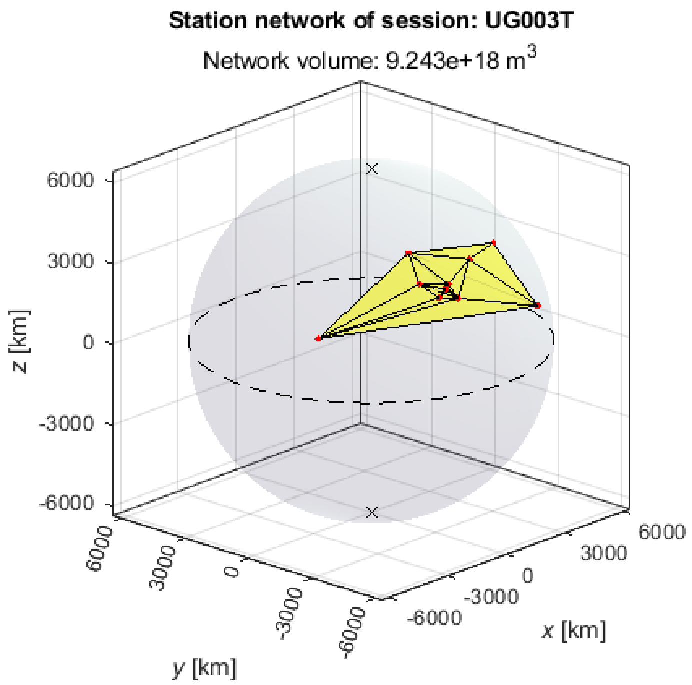

Figure 4.3: A VLBI session (session code UG003T) using the entire network of ten VLBA stations.

This array of VLBI stations was excluded because it was thought that a network like this would pull the TRF towards one direction, despite being a large network. A strictly European network of stations would most likely behave similarly, but because the VLBA consists of ten practically identical stations, and because internally all ten stations are listed under a single identifier, it was very convenient to exclude this network. For completeness, the details and identifiers of each station in the VLBA network can be found in Table 4.3.

Table 4.3: IVS identifiers for the VLBA network and its ten stations. When running ASCOT all stations can be excluded by the IVS station name ”VLBA”.

IVS Code	IVS Station name	DOMES	CDP	Comments/description
Va	VLBA	———	—-	VLBA, all 10 stations:
Br	BR-VLBA	40473S001	7614	VLBA at Brewster, WA, USA
Fd	FD-VLBA	40442S017	7613	VLBA at Ft. Davis, TX, USA
Hn	HN-VLBA	40471S001	7618	VLBA at Hancock, NH, USA
Kp	KP-VLBA	40466S001	7610	VLBA at Kitt Peak, AZ, USA
La	LA-VLBA	40463S001	7611	VLBA at Los Alamos, NM, USA
Mk	MK-VLBA	40477S001	7617	VLBA at Mauna Kea, HI, USA
NL	NL-VLBA	40465S001	7612	VLBA at North Liberty, IA, USA
Ov	OV-VLBA	40439S006	7616	VLBA at Owens Valley, CA, USA
Pt	PIETOWN	40456S001	7234	VLBA at Pie Town, NM, USA
Sc	SC-VLBA	43201S001	7615	VLBA at St. Croix, VI, USA

5

Results

This chapter includes the results from the studies that were conducted to investigate possible causes for the VLBI scale behaviour. First the individual OSO solution that was sent to the IVS is presented, along with the reprocessed solution using ASCOT. These solutions are considered our benchmarks, and any results from the other studies are compared to the estimated drifts and offsets from these solutions, or from the ITRF solutions by Altamimi et al.

The results from each study are presented alongside plots to visualise how the scale has been affected during the *good* and *bad* time periods, respectively. Precise time spans and drift values are found in tables, where the values considered most significant have been highlighted. Additionally, full time series of all seven Helmert parameters, as well as time series from all simulations and reprocessed solutions, can be found in Appendices A, B, and C.

5.1 The Main OSO Solution

First, let us take a look at the OSO solution that was submitted to the IVS combination ($\mathrm{OSO_{IVS}}$) for the ITRF2020. We should note that out of the 6932 available sessions, only 5849 remain at this point. All sessions with fewer than three stations common to the ITRF2014 have been excluded since they would yield a rank deficient system of equations to estimate the seven Helmert parameters. From the remaining sessions and scale factors, outliers have been removed based on a threshold of three scaled median absolute deviations (MAD) away from the median. The remaining 5849 scale factors can be seen in Figure 5.1, where both the *good* and *bad* time periods have been highlighted. The full time series for all seven Helmert parameters can be found in Appendix A.

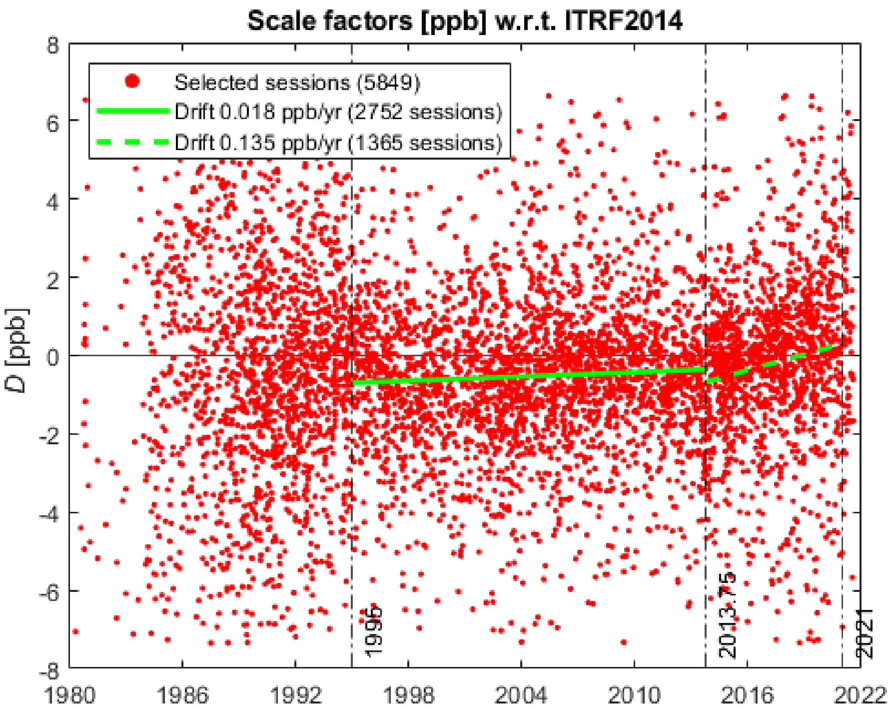

Figure 5.1: Scale factors of the OSO_{IVS} solution. The drift in the time period between 1995.00 to 2013.75 is in line with the observed scale rate, while the scale drift from 2013.75 to 2021.00 is significantly higher.

Having highlighted each region, the scale drift was estimated as a linear non-weighted regression line of all scale factors within each period (including the lower bound, but excluding the upper bound). From the OSO solution we found that the period between 1995.00-2013.75 experienced a drift of 0.018 ppb/yr, while the period between 2013.75-2021.00 experienced a drift of 0.135 ppb/yr. The drift of 0.018 ppb/yr was similar to the observed scale rate of 0.00 ± 0.03 ppb/yr between the ITRF2020 and the ITRF2014. The mean values within the two regions were -0.523 ppb and -0.212 ppb, respectively. Similarly, this was comparable to the previously observed offset of $D = -0.42 \pm 0.03$ between the two ITRFs[1] for the first period.

The second set of data to look at is the reprocessed OSO solution (OSO_{REP}) over the period 2013.75-2021.00, containing 1498 sessions at the start. Sessions were then removed on the basis of having too few stations (less than three), and scale outliers were removed at a three MAD threshold, resulting in 1295 remaining sessions. However, because this solution would only be used as a benchmark and comparison to the other reprocessed solutions, any sessions that had been removed from any of the reprocessed solutions were also removed. Sometimes during the ASCOT processing there are too few observations with the remaining baselines, and ASCOT cannot solve for a TRF and no SINEX file is created either. A linear non-weighted

[1]For a full list of all Helmert parameters between every set of past ITRFs, visit `https://itrf.ign.fr/en/solutions/transformations`.

regression line was estimated for the remaining 1090 sessions in the period between 2013.75 to 2021.00. The drift and mean values were 0.141 ppb/yr and −0.201 ppb, respectively. The time series for these scale factors can be seen in Figure 5.2.

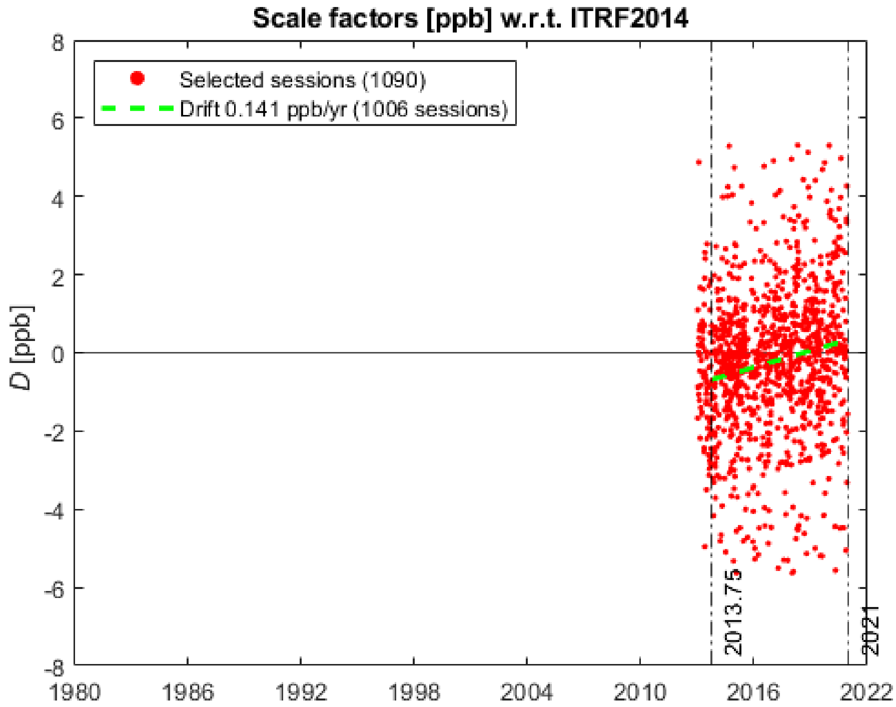

Figure 5.2: Scale factors of the reprocessed OSO_{REP} solution, having removed outliers and sessions that do not appear in all five reprocessed solutions.

The drift from the OSO_{IVS} time series was used as a benchmark during the experiment of artificially adding uplift, while the reprocessed solution OSO_{REP} was used as the benchmark for comparison with the other reprocessed solutions (excluded stations). The benchmarks for the drifts and mean values of each solution and time period can be found in Table 5.1.

Table 5.1: Benchmarks for comparison of each scale drift for the two solutions OSO_{IVS} and OSO_{REP}. During the time span 1995.00-2013.75 the drift and mean value behave as expected, while for the time span 2013.75-2021.00 the drift is significantly higher.

Scale factors	Time span	# of sessions	Drift [ppb/yr]	Mean [ppb]
OSO_{IVS}	1995.00-2013.75	2752	$\mathbf{0.018 \pm 0.007}$	−0.523
OSO_{IVS}	2013.75-2021.00	1365	$\mathbf{0.135 \pm 0.028}$	−0.212
OSO_{REP}	2013.75-2021.00	1006	$\mathbf{0.141 \pm 0.029}$	−0.201

5.2 Impact of Simulated Uplift

Next follow the results of having added some artificial uplift to each of the three stations NYALES20, KOKEE, and HOBART26 (see Table 4.1). Uplift was added so that the drift in the *good* time span of 1995.00-2013.75 would behave similarly to that of the *bad* time span 2013.75-2021.00. An example of how the scale was impacted by the added uplift to the NYALES20 station can be seen in Figure 5.3. The blue dots in the plot indicate how many sessions included the NYALES20 (CDP number 7331) station.

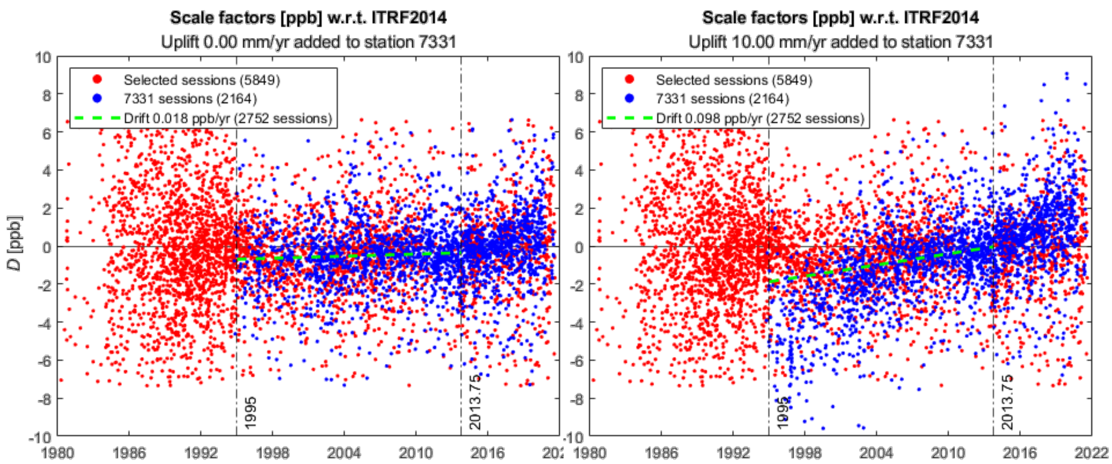

Figure 5.3: Example of what happens when artificial uplift is added to a station. To the left no uplift has been added, but on the right a vertical motion of 10 mm/yr has been added to station 7331 (NYALES20), and the scale drift has increased.

Trial-and-error was used to find an artificial uplift that caused each station to "drag" the scale drift to the bad rate of approximately 0.135 ppb/yr. Because the number of sessions a station appears in (number of blue dots in the figure) varies greatly, the results seemed to reflect that each of the stations impacted the scale drift differently. Nonetheless, all of the stations did have an impact on the scale drift when an artificial uplift was added. The applied uplift rate to the stations were 14.60 mm/yr for NYALES20, 6.85 mm/yr for KOKEE, and 41.40 mm/yr to HOBART26. These results are highlighted in Table 5.2 along with their respective scale drifts and errors. The corresponding plots can be found in Appendix B.

Table 5.2: The artificial uplifts that were added to each station to achieve the same drift rate of approximately 0.135 ppb/yr during the *good* time period.

Simulated	Uplift [mm/yr]	Time span	Drift [ppb/yr]	Mean [ppb]
None	0	1995.00-2013.75	0.018 ± 0.007	-0.523
NYALES20	**14.60**	1995.00-2013.75	0.135 ± 0.009	-1.126
KOKEE	**6.85**	1995.00-2013.75	0.135 ± 0.008	-1.179
HOBART26	**41.40**	1995.00-2013.75	0.135 ± 0.012	-1.185

Note that all of the artificially added uplifts are very large. While the linear motion of stations is usually given in the order of mm/yr, the actual velocities are are often in the sub-mm range. Hence the values in Table 5.2 are rather unrealistic since mismodeling in uplifts of almost 7, 15, and 41 mm/yr seem highly unlikely. However, the results of this experiment implies that the velocity of a single station could possibly affect the scale of the entire network to a significant degree.

5.3 Station Technical Aspects

Moving forward, this section contains the results of the study when excluding stations from the reprocessed ASCOT solutions ($\mathrm{OSO_{REP}}$ and $\mathrm{OSO_{REP\text{-}STATION}}$), as well as the solution excluding all VLBA sessions (71 sessions). Just like before, these solutions were processed in the same way to determine the Helmert parameters. To estimate the scale drift of each solution, the 1090 sessions included in all reprocessed solutions were used, as discussed in Section 5.1. Compared to the scale drift of approximately 0.141 ppb/yr by the solution with no excluded sessions, the drift actually seemed to improve for both solutions without SEJONG and YEBES40M. As an example, the full solution compared to having excluded SEJONG can be seen in Figure 5.4.

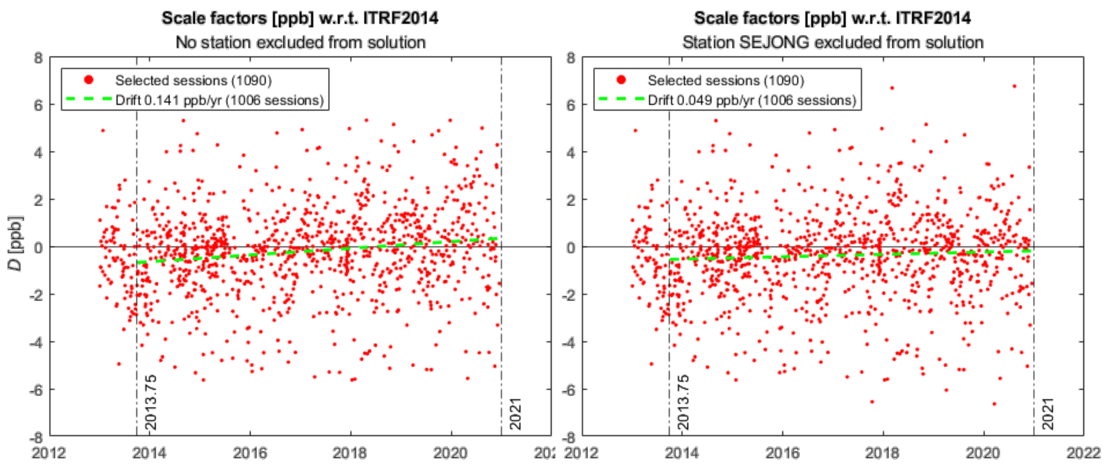

Figure 5.4: Reprocessed scale factors during the time period between 2013.00 to 2021.00. To the left no stations have been excluded from the solution, but to the right the station SEJONG has been excluded entirely. Note how the scale drift appears to flatten.

We found that having excluded SEJONG from the solution, the scale drift decreased to approximately 0.049 ppb/yr and the mean value down to -0.384 ppb. Likewise for the solution without YEBES40M the scale drift decreased to 0.088 ppb/yr and the mean value down to -0.453 ppb. The scale drifts of both solutions decreased well beyond the formal errors of the estimated drifts, getting closer to the observed value of about 0.00 ± 0.03 ppb/yr between the ITRF2020 and ITRF2014. The mean values, or offsets, also seemed to improve by getting closer to the observed value of

-0.42 ± 0.03 ppb. However, none of the solutions without NYALES20 (drift 0.158 ppb/yr, mean -0.101 ppb) and without the VLBA sessions (drift 0.148 ppb/yr, mean -0.192 ppb) saw any significant reductions in the scale drift. Instead the two drifts almost appeared to increase, but they were still withing range of their respective formal errors. The results of this study can be found in Table 5.3, where the most significant numbers have been highlighted in bold.

Table 5.3: Drifts and mean values of all five reprocessed solutions with four solutions having excluded a single station during ASCOT processing. Solutions excluding the stations SEJONG and YEBES40M that both had experienced technical issues seem to have improved the scale drift, while excluding NYALES20 and VLBA almost had the opposite effect.

Scale factors	Time span	# of sessions	Drift [ppb/yr]	Mean [ppb]
OSO_{REP}	2013.75-2021.00	1006	0.141 ± 0.029	-0.201
$OSO_{REP\text{-}NYALES20}$	2013.75-2021.00	1006	0.158 ± 0.031	-0.101
$OSO_{REP\text{-}SEJONG}$	2013.75-2021.00	1006	$\mathbf{0.049 \pm 0.028}$	$\mathbf{-0.384}$
$OSO_{REP\text{-}YEBES40M}$	2013.75-2021.00	1006	$\mathbf{0.088 \pm 0.031}$	$\mathbf{-0.453}$
$OSO_{REP\text{-}VLBA}$	2013.75-2021.00	935	0.148 ± 0.030	-0.192

This experiment seemed to imply that excluding sessions from the solution might impact the scale, for better or for worse. It was interesting that the solutions where stations were excluded based on network volume or distribution (NYALES20 and VLBA) had a slight negative impact on the scale. Worth noting is that the NYALES20 station appeared frequently in 2164 out of the 5849 VLBI sessions over the entire time span. For this station especially, it would intuitively then imply that its presence might help stabilize the network. On the other hand, the slight improvements seen when having removed the two stations affected by technical issues suggest that these technical aspects might have a significant impact on the scale. The full time series of each reprocessed solution, where each of the stations have been excluded, can be found in Appendix C.

5.4 Network Volume and Distribution

Finally, the properties of the VLBI station networks were also studied. The idea was to gain some insight as to how, or if, the TRF scale was affected by the distribution or volume of a network. However, after having excluded the VLBA sessions from the reprocessed solutions without seeing any significant impact, at least it could be concluded that there was no direct connection between that part of the VLBI network evolution and the scale behaviour. Instead a brief study of the network volume evolution for the entire 40+ years of VLBI sessions was conducted.

The first thing to look at is Figure 5.5 showing the time series of network volumes that were used to compute the scale factors from Figure 5.1. While not necessarily showing some obvious connection to the behaviour of the scale factor, it can be noted that the VLBI networks have generally kept growing during the lifetime of the VLBI technique with significantly smaller network volumes prior to 1995.00. It could also be of interest to note that the network volumes appears to have stopped growing around 2014-2015.

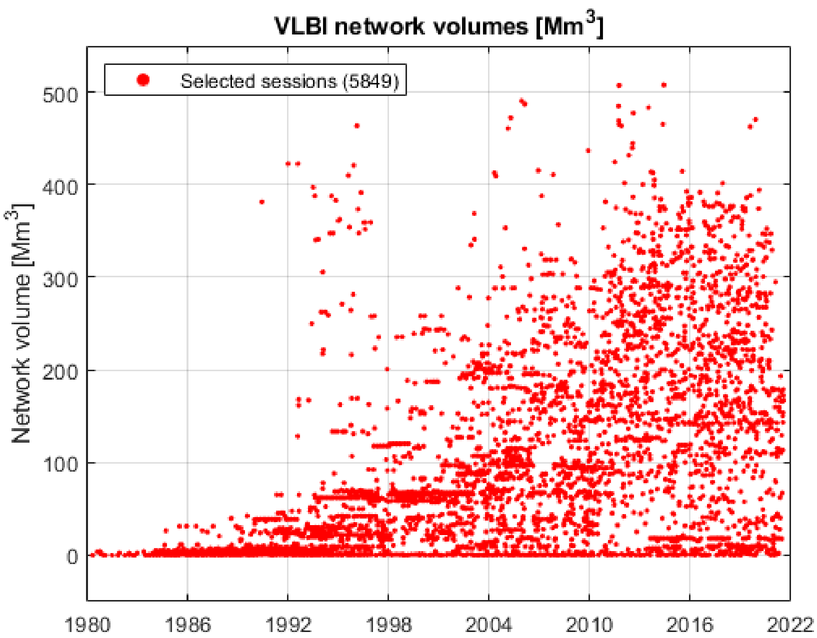

Figure 5.5: The network volume time series of the VLBI sessions used to compute the Helmert parameters. Only stations common to both the OSO TRFs and the ITRF2014 have been accounted for. Note how the growing networks follow the evolution and development of the VLBI networks.

We can also look at the scale factors as a function of network volume, as presented in Figure 5.6. However, there did not appear to be any direct connection between scale and volume. The smallest network volumes appear to experience a bit larger scatter, but the scale does not appear significantly more stable at the largest network volumes. Of course there are also other properties to a network other than volume, suggesting that for instance number of stations or more importantly their distribution might be interesting.

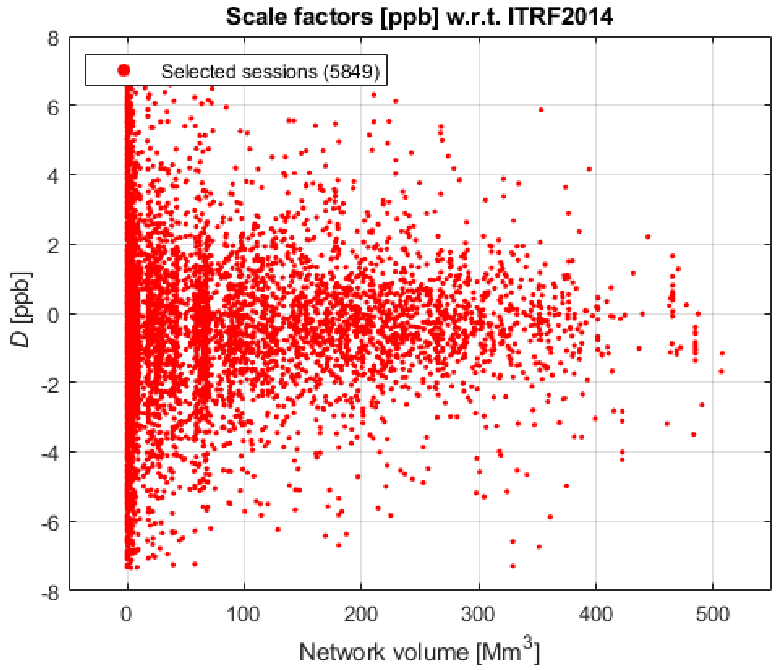

Figure 5.6: Scale factors as a function of network volume. While there is no immediate connection, the smallest networks tend to see the widest distribution of scale factors.

6
Discussion

The strange behaviour of the VLBI scale factor for the ITRF2020 has been acknowledged for instance by Altamimi et al. (2022) and Hellmers et al. (2022). However, as of yet, there does not seem to be a clear cause as to why the scale is behaving that way, and during this project it was made apparent that there was likely not a singular obvious culprit. Nonetheless, this project was carried out to study one possibly aspect that might affect it, and to reiterate the main question of this project, how is the VLBI scale factor affected by the session network components? This chapter will elaborate on the findings, and also point out possible flaws, points for improvements, and ideas for future studies.

First we should acknowledge the first limiting factor about this project, that the analysis performed was limited to the OSO contribution (computed using ASCOT) to the IVS combination. This was seen as something of an issue, since the ITRF scale is actually based on the combined solution from eleven different ACs, using seven different computational software, each of which may apply different constraints or use different files locally. While some access was granted to similar solutions from other ACs, the amount of work necessary to confirm (or disprove) that the scale drift behaviour appeared in multiple solutions was outside the scope of this project. However, as presented by Hellmers et al. (2022), similar behaviour has indeed been noted in essentially all of the contributed solutions to the IVS. The investigation by Hellmers et al. (2022) had looked for some connection between the type of sessions and the scale, but found no significant change between XA/XE sessions. For future work, the MATLAB tools developed during this project could prove useful for similar investigations. Finally was a proposition of continued investigations, especially regarding the weighting of different AC solutions against each other, and according to their software. The software known as Calc/SOLVE is currently in use by five different ACs (unlike ASCOT which is only used by the OSO AC) and is thus in a dominating position for the IVS combined solution. Considering the fact that every AC solution experienced similar behaviour despite using different software, it meant that any findings for the OSO solution could possibly be applied to the other solutions also.

As for the first finding of this project, looking back at Section 5.2, the analysis suggests that even a slight deviation in vertical velocity *for just a single station* could actually impact the scale of a TRF significantly. While the numbers used in this study were of an in practice unreasonable magnitude, this still suggests that some erroneous uplift for a station might have a very real impact. For instance there could maybe be some event, akin to the discontinuities discussed in Section 2.4.3, that happened somewhere around the epoch 2014.00 but which has not been accounted for properly.

The uplift simulation comes with one unresolved flaw, however. The linear regression model used to fit the data in each time period was non-weighted, that is to say that the standard deviations of the scale factors were not used as weights for the solution. Ideally these would be applied like the inverse variance in Section 3.1. However, when adding uplift to a station it was noted that the standard deviation also changed substantially. For reference, the standard deviations corresponding to the scale factors in Figure 5.3 can be seen in Figure 6.1, where blue dots once again mark the sessions where uplift has been added to the station NYALES20.

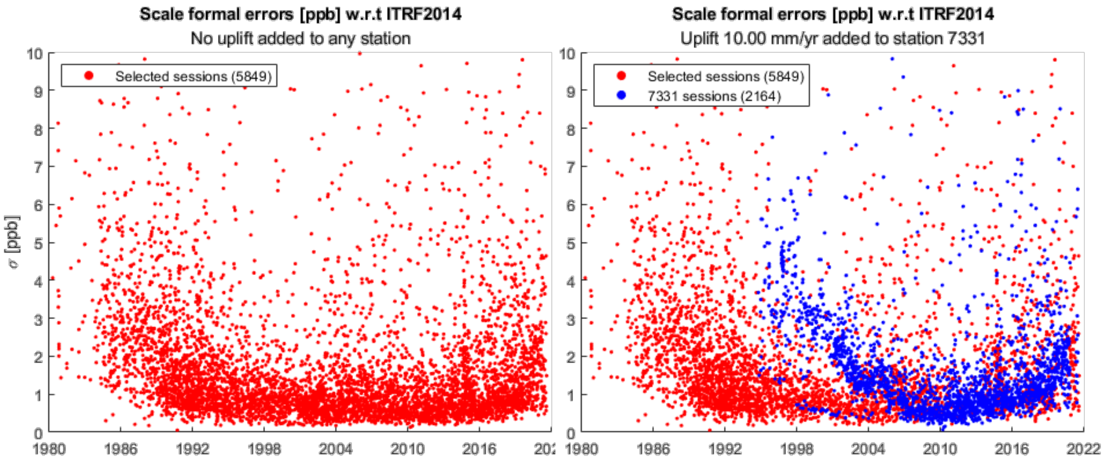

Figure 6.1: Standard deviations σ of the OSO_{IVS} scale factors. The left plot corresponds to the time series of the IVS contribution, note the increasing lower threshold in recent years. The right plot includes the artificial uplift of 10 mm/yr added to station 7331 (NYALES20) marked in blue, notice how a similar lower threshold can be observed farther back in time too.

The left plot also corresponds to the standard deviations of the scale factors in Figure 5.1, that is the entire OSO_{IVS} solution. Ignoring the values before 1995, the left plot shows that the standard deviations are also starting to drift upwards beginning around 2015-2016. This of course gives some substance to the claim that the scale does indeed appear to be drifting. Furthermore, when artificial uplift was added to a station (in this case 10 mm/yr to NYALES20), similar behaviour can be seen all over the time series, here the affected sessions are marked in blue. With more time for the project, this would likely have been the next major point of investigation as this was deemed quite peculiar. However, in the case of linearly fitting a drift with these values as weights (inverse squared), the increased standard deviations reduced the impact of every session with added uplift to the point where the drift was barely affected. But judging by Figure 5.3 that was clearly not the case, the scale was evidently showing similar behaviour as that which laid the foundation of this project.

The next point of discussion will be the connection between the scale factor and the VLBI network properties, mainly concerning network volume. While this study was interesting in the context of the evolution of the VLBI technique, it did not provide any direct connections to the scale drift. However, it should be noted that Altamimi et al. (2022) seems to have imposed a new constraint regarding volume when selecting VLBI sessions for the scale contribution of the ITRF2020, that is each session had a network volume of $\geq 10^{19}$ m^3 (or ≥ 10 Mm^3). During this study, the addition of such a threshold was implemented, but it did not yield any significant results, except for removing a number of sessions, as seen in Figure 5.5 and 5.6. However, the idea that the scale is impacted by the network volume or distribution seems intuitively to be on the right track, and more extensive studies might prove beneficial for the future. Especially considering the fact that major development of the VLBI networks, for instance the deployment of the next generation VLBI system VGOS has also happened in recent years. Because of this, many of the VGOS stations had not yet been added as reference points to the ITRF as of version ITRF2014, but they do appear in the ITRF2020.

For the last point we will discuss what might perhaps have been the most significant results, that is regarding the exclusion of specific VLBI stations. The major flaw with this study was the low number of reprocessed solutions with excluded stations. Unfortunately, this was purely due to time constraints of the project. However, the preliminary results did suggest that excluding stations suffering from some technical issues may have a positive impact on the scale behaviour. When reprocessing the global solutions using ASCOT, it was also noted that some stations were missing meteorological data. The ASCOT software handled this error using some default values, but this also begs the question whether other models might also provide strange results, and how widespread such an issue would be. Future work could focus on further investigations regarding other models, such as thermal and gravitational deformations of antennas, or geophysical models for other atmospheric corrections and pressure loading.

On the topic of continued investigations, the exclusion of the station YEBES40M with its sub-reflector discontinuity implied some interesting results. A next step could be to identify stations with potential position mismodeling like NYALES20, or perhaps to systematically exclude each of the 33 stations affected by discontinuities. Out of those, the thirteen stations with PSD corrections to their trajectories could perhaps be skipped at first, since Altamimi et al. (2016) has shown that the GNSS-fitted models follow the station motions very well. A more extensive list of stations with technical data and correlation issues like SEJONG might also prove useful, to avoid having to blindly exclude each of the 154 stations in the ITRF2014.

This wraps up the discussion chapter, with some flaws regarding methods have been pointed out. Perhaps more interesting are the ideas regarding future investigations. Since no clear cause for the scale drift behaviour has been observed yet, the prospects of finding a solution are exciting to say the least.

7
Conclusion

During this project we have found that the individual OSO solution which enters into the IVS combined solution, and by extension the ITRF solution, seems to experience the scale drift behaviour. However, it should be reiterated that this work was based on the ITRF2014 as the reference frame for comparison, and not the latest ITRF2020. Perhaps implementing the ITRF2020 into this work, and performing the same studies could prove insightful, considering the fact that the ITRF2020 was published despite the VLBI scale behaviour still not having been resolved. Additionally, during this project we have been limited to the individual OSO solution. We therefore propose further investigations into both individual solutions from other ACs as well as the IVS combined solution.

Perhaps more importantly, our preliminary results suggest that there is not just a single reason for the VLBI scale behaviour. Instead the scale drift appears to be a result of a combination of factors, ranging from technical issues with specific VLBI stations, the possible use of erroneous station motion models, or as suggested during the ASCOT VLBI data analysis, the use (or lack of) different geophysical models. We saw that excluding specific VLBI stations from a solution may decrease the scale drift, while removing others have the opposite effect. We also saw significant scale drift in VLBI sessions where just a single station had an artificial uplift added. The added values were possibly too large in magnitude to be considered feasible, however.

Especially future work regarding the properties of an entire VLBI session would be interesting, rather than focusing on its components. We still heavily suspect that there is further insight to be gained from studying the entire network volume and its geographical distribution. Perhaps the same could also be applicable to the other space-geodetic techniques. However, not enough time was allocated to that specific subject during this project and no direct connection was found.

While this work is in need of further validation, it might certainly prove useful in future investigations, some of which have been proposed here. As a concluding remark, we are looking forward to see the results of future studies regarding the VLBI scale behaviour. There are various other aspects to consider, and, if nothing else, we can conclude that the problem appears far more complex than one might initially expect.

Bibliography

Altamimi, Z., D. Angermann, D. Argus, et al. (2001). “The terrestrial reference frame and the dynamic Earth”. In: *Eos, Transactions American Geophysical Union* 82.25, pp. 273–279. DOI: `https://doi.org/10.1029/EO082i025p00273-01`. eprint: `https://agupubs.onlinelibrary.wiley.com/doi/pdf/10.1029/EO082i025p00273-01`. URL: `https://agupubs.onlinelibrary.wiley.com/doi/abs/10.1029/EO082i025p00273-01`.

Altamimi, Z., P. Rebischung, X. Collilieux, et al. (2022). “ITRF2020: main results and key performance indicators”. In: EGU General Assembly 2022 (Vienna, Austria, May 23, 2022). DOI: `https://doi.org/10.5194/egusphere-egu22-3958`.

Altamimi, Z., P. Rebischung, L. Metivier, et al. (2017a). “The International Terrestrial Reference Frame: lessons from ITRF2014”. In: *Rendiconti Lincei. Scienze Fisiche e Naturali* 29, pp. 23–28. DOI: `10.1007/s12210-017-0660-9`.

Altamimi, Z., P. Rebischung, L. Métivier, et al. (2016). “ITRF2014: A new release of the International Terrestrial Reference Frame modeling nonlinear station motions”. In: *Journal of Geophysical Research: Solid Earth* 121.8, pp. 6109–6131. DOI: `https://doi.org/10.1002/2016JB013098`. eprint: `https://agupubs.onlinelibrary.wiley.com/doi/pdf/10.1002/2016JB013098`. URL: `https://agupubs.onlinelibrary.wiley.com/doi/abs/10.1002/2016JB013098`.

Altamimi, Z., P. Rebischung, L. Métivier, et al. (2017b). *Analysis and results of ITRF2014 (IERS Technical Note No. 38)*. URL: `https://www.iers.org/IERS/EN/Publications/TechnicalNotes/tn38.html`.

Angermann, D., M. Seitz, and H. Drewes (2013). “Global Terrestrial Reference Systems and Their Realizations”. In: *Sciences of Geodesy - II: Innovations and Future Developments*. Ed. by G. Xu. Berlin, Heidelberg: Springer Berlin Heidelberg, pp. 97–132. ISBN: 978-3-642-28000-9. DOI: `10.1007/978-3-642-28000-9_3`. URL: `https://doi.org/10.1007/978-3-642-28000-9_3`.

Artz, T., S. Halsig, A. Iddink, et al. (2016). “ivg::ASCOT: Development of a New VLBI Software Package”. In: *New Horizons with VGOS*. Ed. by D. Behrend, K. D. Baver, and K. L. Armstrong, pp. 217–221.

Bachmann, S., L. Messerschmitt, and D. Thaller (2017). “IVS Contribution to ITRF2014”. In: *REFAG 2014*. Ed. by Tonie van Dam. Cham: Springer International Publishing, pp. 47–52. ISBN: 978-3-319-45629-4.

Behrend, D. (2013). “Data Handling within the International VLBI Service”. In: vol. 12. DOI: `http://doi.org/10.2481/dsj.WDS-011`.

Bruyninx, C., Z. Altamimi, E. Brockmann, et al. (2017). “Implementation of the ETRS89 in Europe: Current Status and Challenges”. In: *REFAG 2014*. Ed. by

T. van Dam. Cham: Springer International Publishing, pp. 135–145. ISBN: 978-3-319-45629-4.

Charlot, P., C. S. Jacobs, D. Gordon, et al. (2020). “The third realization of the International Celestial Reference Frame by very long baseline interferometry”. In: *Astronomy & Astrophysics* 644, A159. DOI: 10.1051/0004-6361/202038368. URL: https://doi.org/10.1051/0004-6361/202038368.

Heinkelmann, R. (2013). “VLBI Geodesy: Observations, Analysis and Results”. In: *Geodetic Sciences*. Ed. by S. Jin. Rijeka: IntechOpen. Chap. 3. DOI: 10.5772/54446. URL: https://doi.org/10.5772/54446.

Hellmers, H., S. Modiri, S. Bachmann, et al. (2022). “Evaluation of the IVS contribution to the ITRF2020”. In: EGU General Assembly 2022 (Vienna, Austria, May 23, 2022). DOI: https://doi.org/10.5194/egusphere-egu22-5116.

International VLBI Service for Geodesy & Astrometry (2022). *Data and Products Overview*. URL: https://ivscc.gsfc.nasa.gov/products-data/index.html (visited on 01/20/2022).

Jivall, L. and M. Lidberg (2000). “SWEREF 99 - an Updated EUREF Realisation for Sweden”. In: EUREF symposium 2000.

Johnson, M. C., A. Fey, B. Dorland, et al. (2019). “Half the Time: An Overview of the LBO-USNO Timeshare Agreement”. In: *International VLBI Service for Geodesy and Astrometry 2018 General Meeting Proceedings: ”Global Geodesy and the Role of VGOS - Fundamental to Sustainable Development*, pp. 128–130. URL: https://ivscc.gsfc.nasa.gov/publications/gm2018/28_johnson_etal.pdf.

Malys, Stephen, Russell Solomon, Jason Drotar, et al. (2021). “Compatibility of Terrestrial Reference Frames used in GNSS broadcast messages during an 8 week period of 2019”. In: *Advances in Space Research* 67.2, pp. 834–844. ISSN: 0273-1177. DOI: https://doi.org/10.1016/j.asr.2020.11.029. URL: https://www.sciencedirect.com/science/article/pii/S0273117720308292.

MATLAB version 9.11.0.1873467 (R2021b) Update 3 (2021). The Mathworks, Inc. Natick, Massachusetts.

Nilsson, T. and R. Haas (2010). “Impact of atmospheric turbulence on geodetic very long baseline interferometry”. In: *Journal of Geophysical Research* 115, pp. 1–11.

Nilsson, T., J. A. Mora-Diaz, V. Raposo-Pulido, et al. (2017). “Antenna Axis Offsets and Their Impact on VLBI Derived Reference Frames”. In: *REFAG 2014*. Ed. by T. van Dam. Cham: Springer International Publishing, pp. 53–58. ISBN: 978-3-319-45629-4.

Nothnagel, A., T. Artz, D. Behrend, et al. (2017). “International VLBI Service for Geodesy and Astrometry”. In: *Journal of Geodesy* 91 (7), pp. 711–721. DOI: 10.1007/s00190-016-0950-5. URL: https://doi.org/10.1007/s00190-016-0950-5.

Petit, G and B Luzum (2010). *IERS Conventions (2010) (IERS Technical Note ; 36)*. 179 pp.

Poyard, J.-C., X. Collilieux, J.M. Muller, et al. (2020). *IGN best practice for surveying instrument reference points at ITRF co-location sites (IERS Technical Note ; 39)*. 167 pp. URL: https://www.iers.org/IERS/EN/Publications/TechnicalNotes/tn40.html?nn=94912.

Robertson, Douglas S. (1991). “Geophysical applications of very-long-baseline interferometry”. In: *Rev. Mod. Phys.* 63 (4), pp. 899–918. DOI: 10.1103/RevModPhys.63.899. URL: https://link.aps.org/doi/10.1103/RevModPhys.63.899.

Schuh, H. and D. Behrend (2012). “VLBI: A fascinating technique for geodesy and astrometry”. In: *Journal of Geodynamics* 61, pp. 68–80. DOI: 10.1016/j.jog.2012.07.007.

Schuh, H. and J. Böhm (2013). “Very Long Baseline Interferometry for Geodesy and Astrometry”. In: *Sciences of Geodesy - II: Innovations and Future Developments*. Ed. by G. Xu. Berlin, Heidelberg: Springer Berlin Heidelberg, pp. 339–376. ISBN: 978-3-642-28000-9. DOI: 10.1007/978-3-642-28000-9_7. URL: https://doi.org/10.1007/978-3-642-28000-9_7.

Soffel, M. and R. Langhans (2013). *Space-Time Reference Systems*. Berlin: Springer. ISBN: 978-3-642-30226-8. DOI: https://doi.org/10.1007/978-3-642-30226-8.

Vestøl, O., J. Ågren, H. Steffen, et al. (2019). “NKG2016LU: a new land uplift model for Fennoscandia and the Baltic Region”. In: *Journal of Geodesy* 93, pp. 1759–1779. DOI: 10.1007/s00190-019-01280-8. URL: https://doi.org/10.1007/s00190-019-01280-8.

A

OSO_{IVS} Helmert Parameters

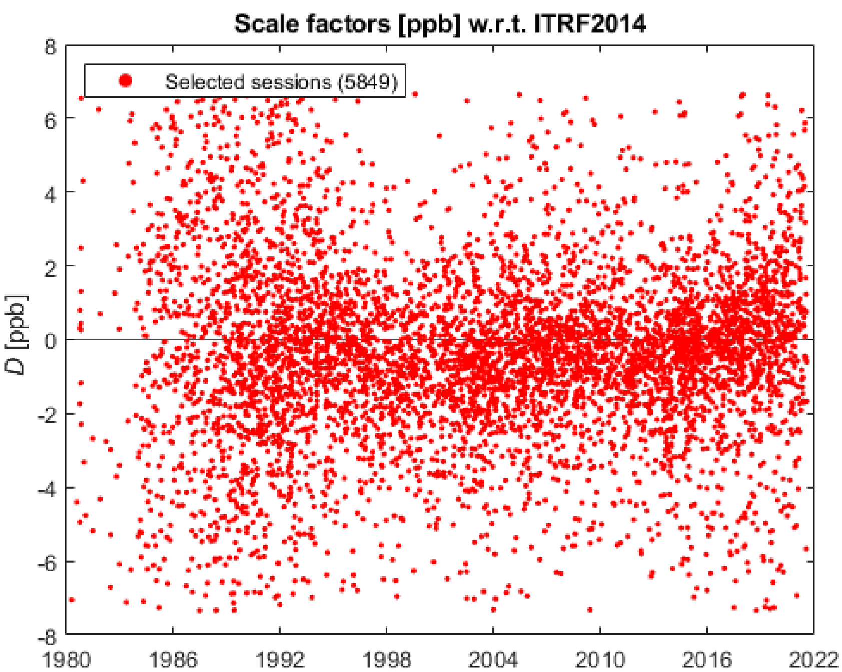

Figure A.1: Full time series of scale factors D from the OSO solution that was submitted to the IVS combination.

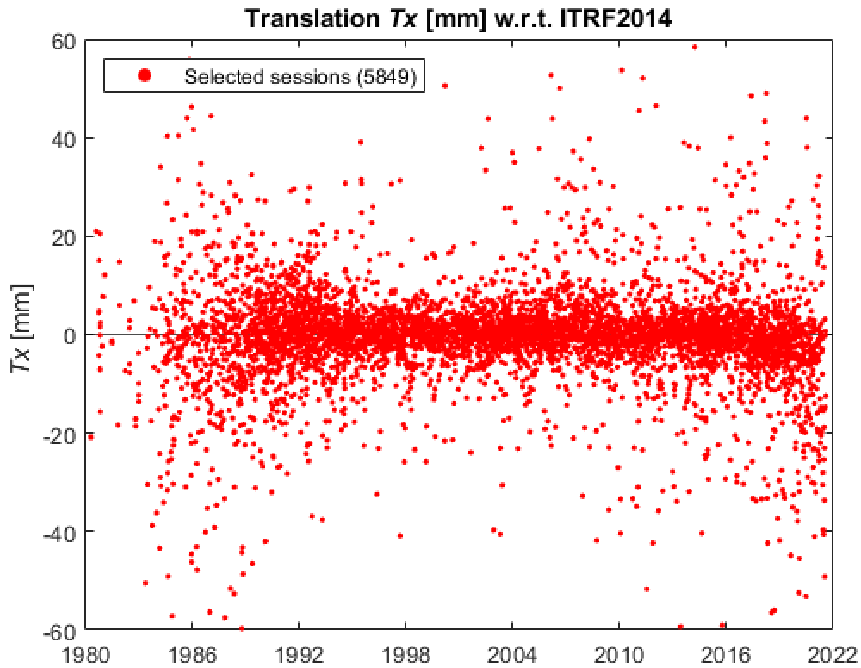

Figure A.2: Full time series of translation parameters T_x from the OSO solution that was submitted to the IVS combination.

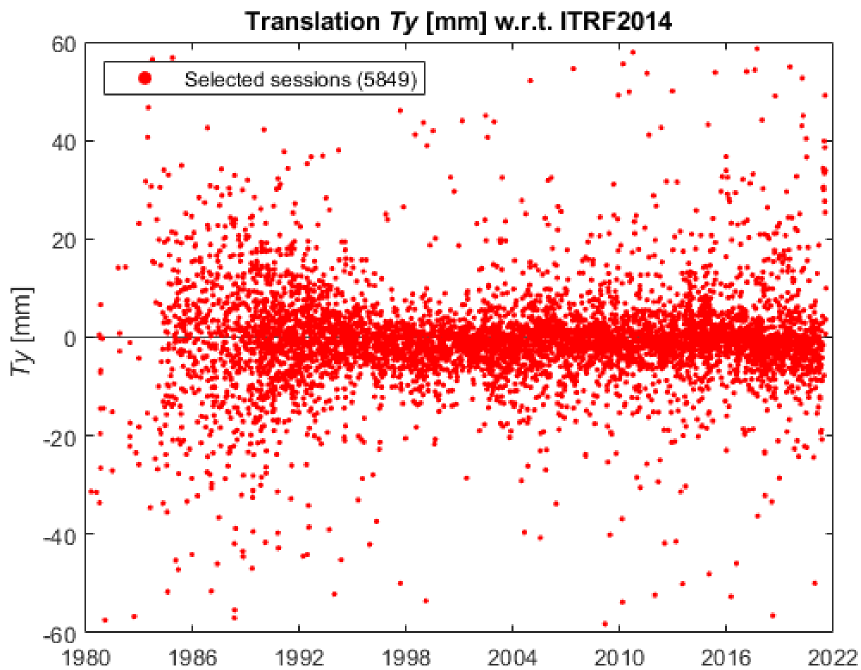

Figure A.3: Full time series of translation parameters T_y from the OSO solution that was submitted to the IVS combination.

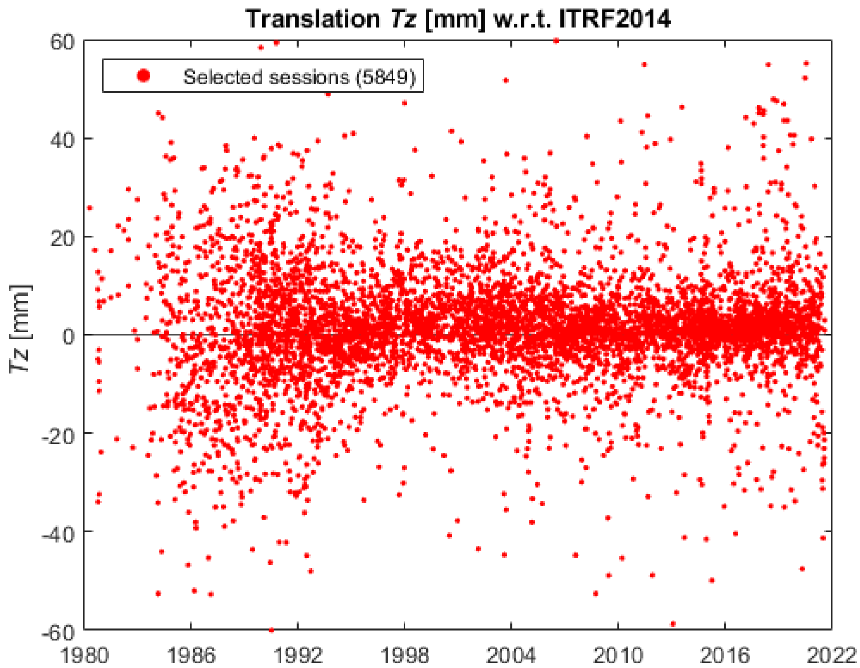

Figure A.4: Full time series of translation parameters T_z from the OSO solution that was submitted to the IVS combination.

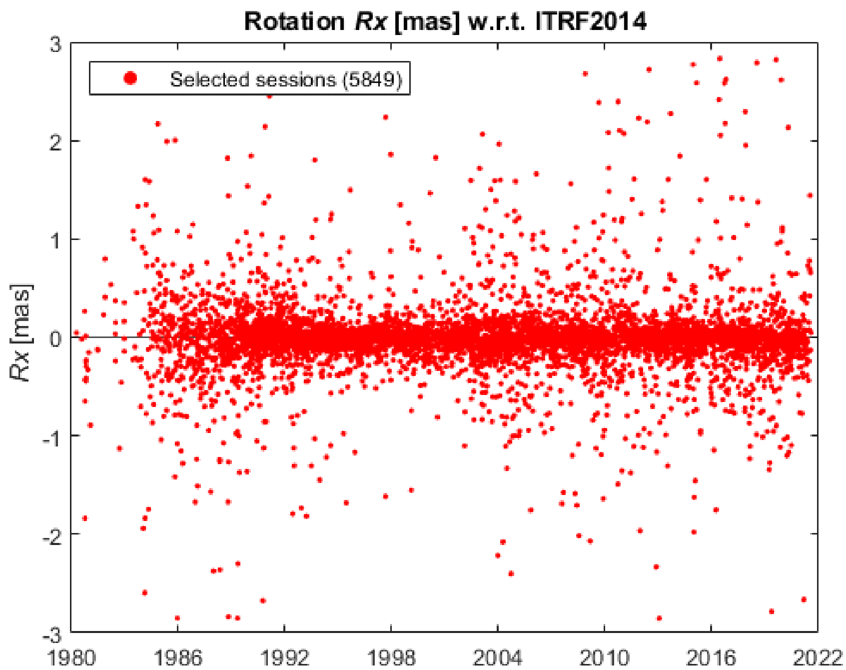

Figure A.5: Full time series of rotation angles R_x from the OSO solution that was submitted to the IVS combination.

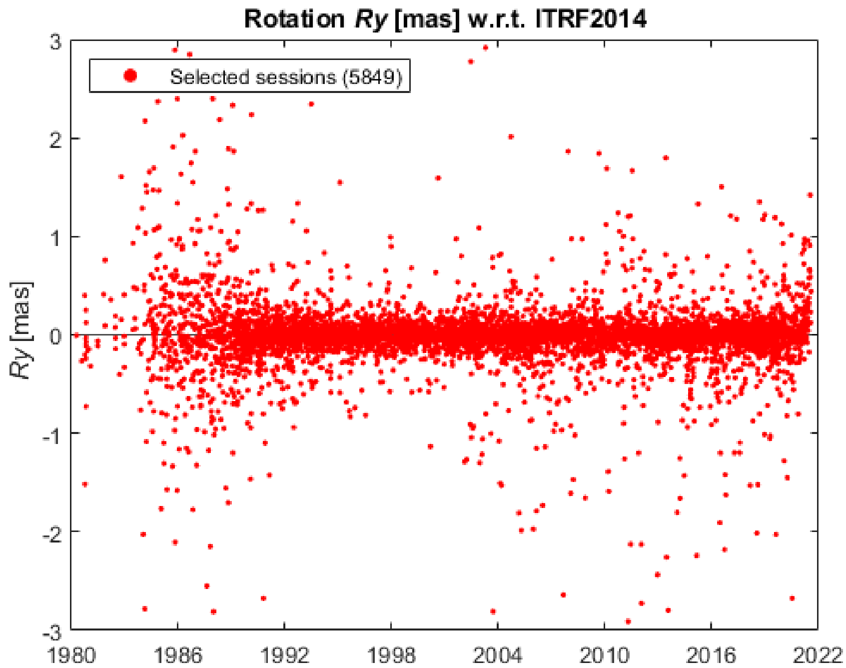

Figure A.6: Full time series of rotation angles R_y from the OSO solution that was submitted to the IVS combination.

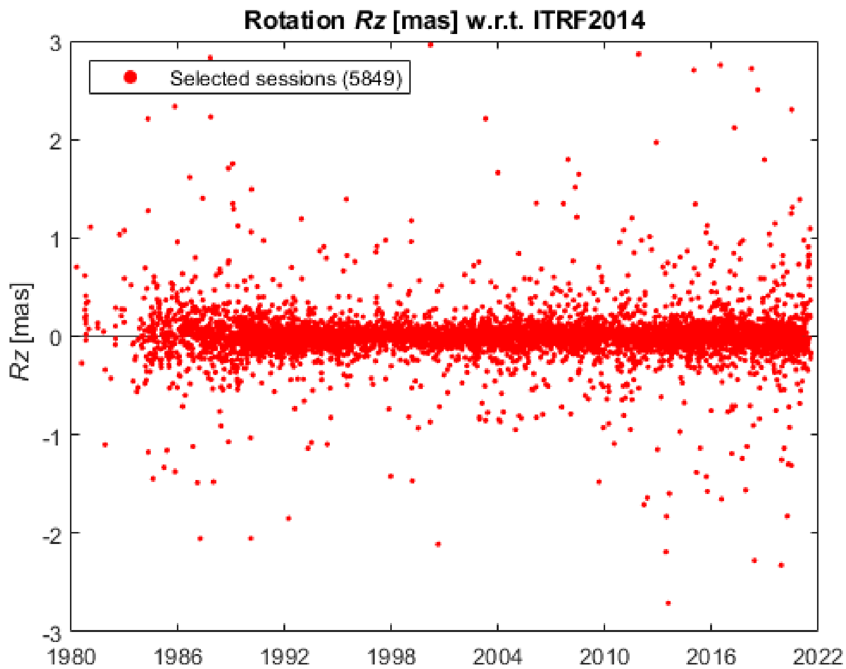

Figure A.7: Full time series of rotation angles R_z from the OSO solution that was submitted to the IVS combination.

B

Simulated Uplift

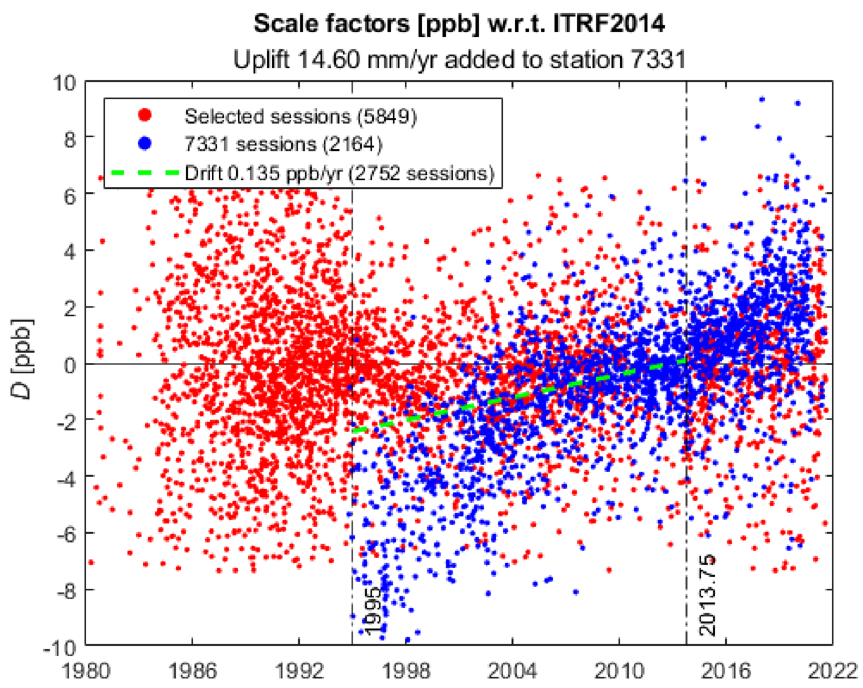

Figure B.1: Added uplift of 14.60 mm/yr to station NYALES20 to achieve a scale drift of approximately 0.135 ppb/yr in the period 1995.00 to 2013.75.

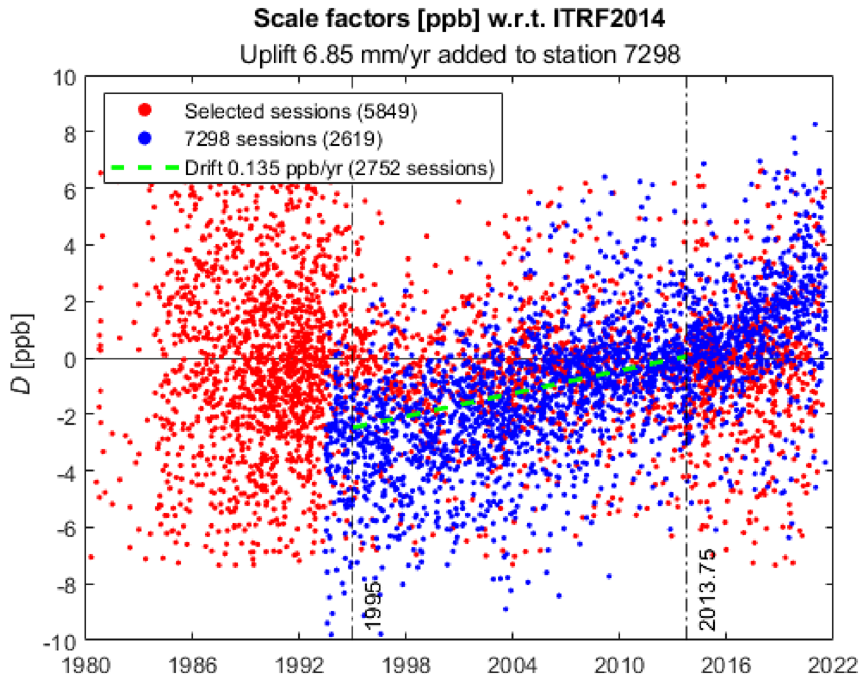

Figure B.2: Added uplift of 6.85 mm/yr to station KOKEE to achieve a scale drift of approximately 0.135 ppb/yr in the period 1995.00 to 2013.75.

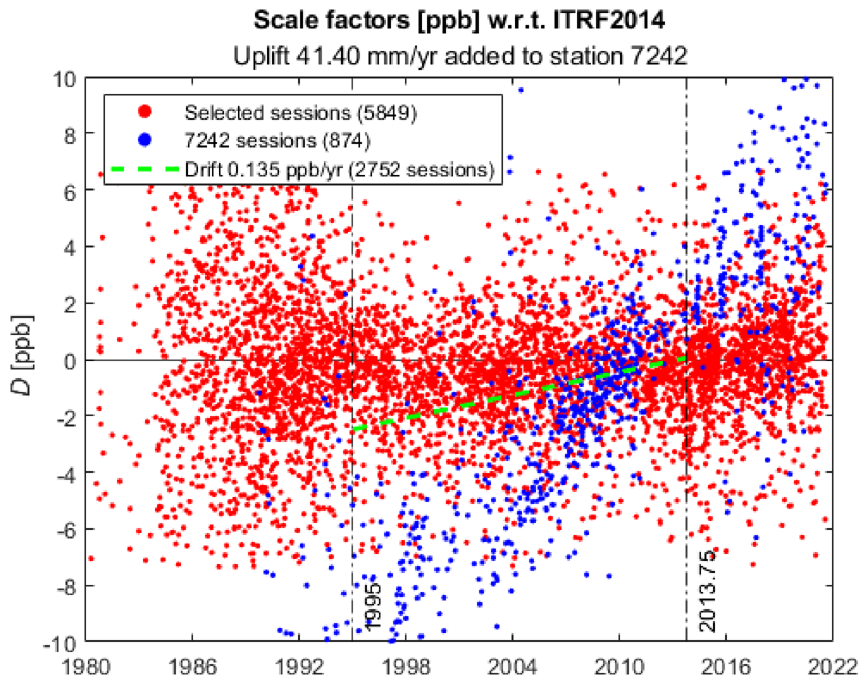

Figure B.3: Added uplift of 41.40 mm/yr to station HOBART26 to achieve a scale drift of approximately 0.135 ppb/yr in the period 1995.00 to 2013.75.

C

Reprocessed ASCOT Solutions

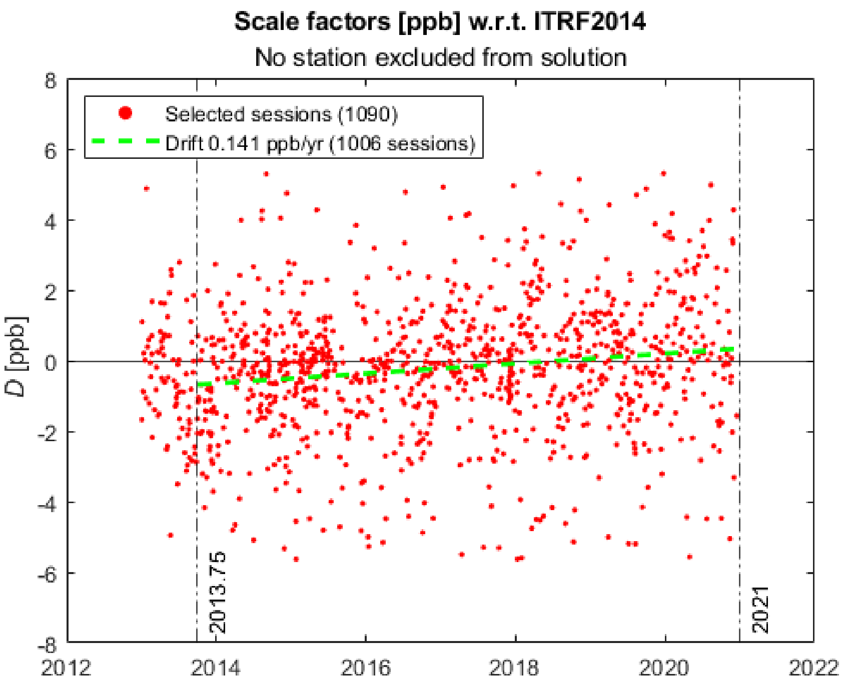

Figure C.1: Reprocessed global solution for VLBI sessions between 2013.00 to 2021.00, including all stations.

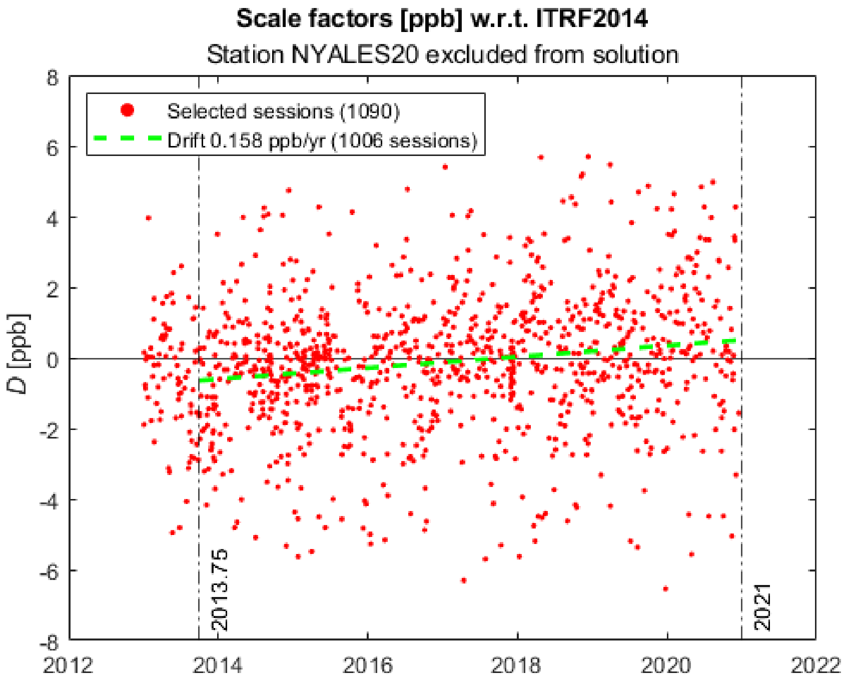

Figure C.2: Reprocessed global solution for VLBI sessions between 2013.00 to 2021.00, having excluded the station NYALES20.

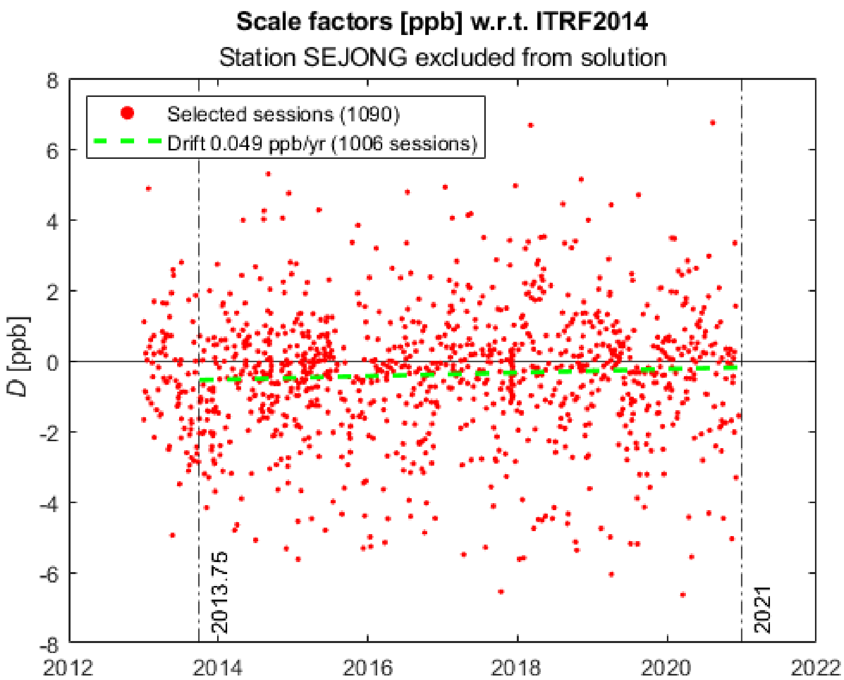

Figure C.3: Reprocessed global solution for VLBI sessions between 2013.00 to 2021.00, having excluded the station SEJONG.

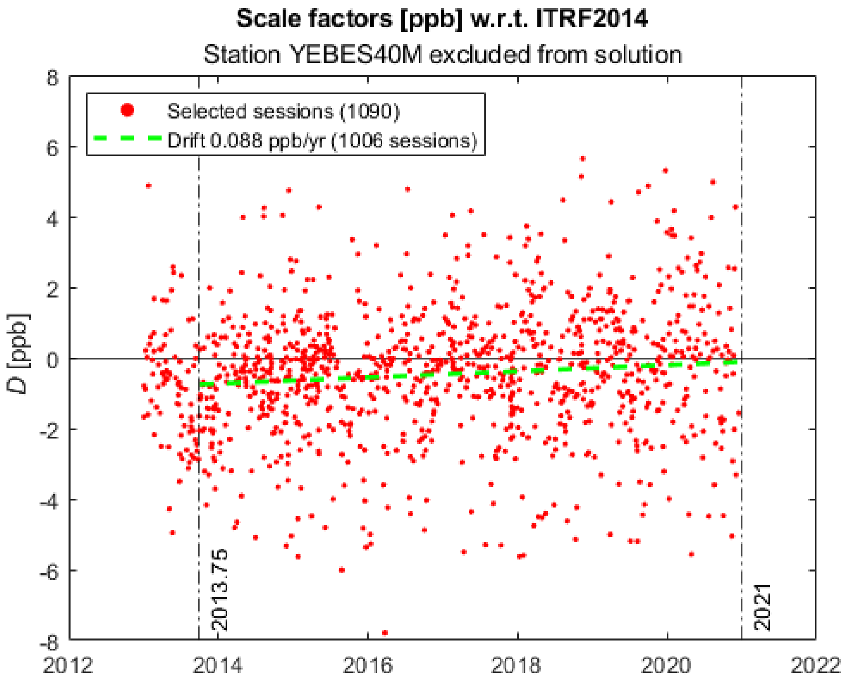

Figure C.4: Reprocessed global solution for VLBI sessions between 2013.00 to 2021.00, having excluded the station YEBES40M.

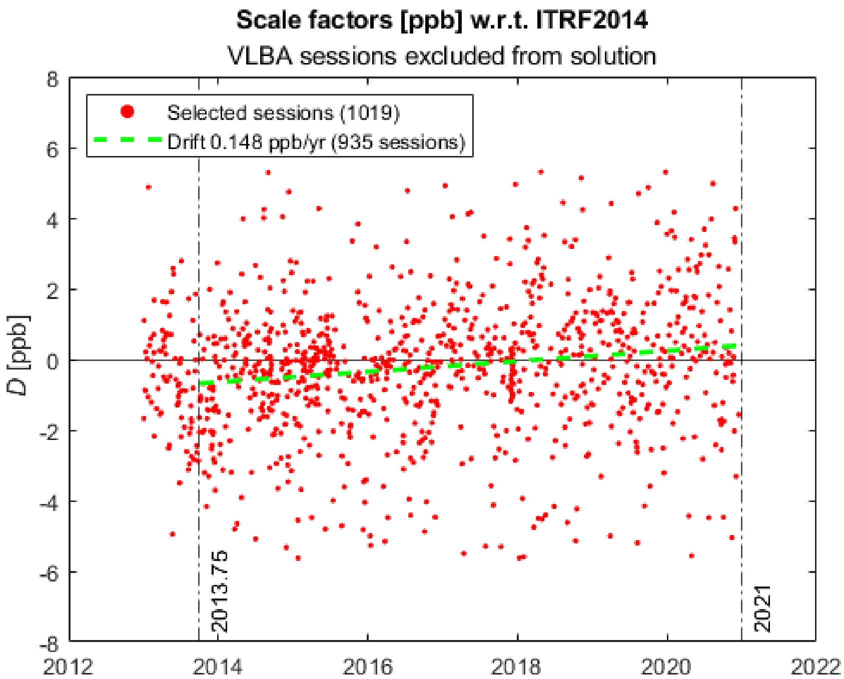

Figure C.5: Reprocessed global solution for VLBI sessions between 2013.00 to 2021.00, having excluded all sessions using only the VLBA network.

DEPARTMENT OF SPACE, EARTH AND ENVIRONMENT
CHALMERS UNIVERSITY OF TECHNOLOGY
Gothenburg, Sweden
www.chalmers.se

AVANCEZ
1829

CHALMERS
UNIVERSITY OF TECHNOLOGY